4 Reliability Analysis of Hyperbolic Paraboloid Shaped TMS

4.1 General

The main source of motivation for this part of thesis have come from the curiosity of understanding the behavior of such a non-conventional, unorthodox, non-linear structures, and also from the willingness of exploring some design limitations to contribute to the close to real visualization of a TMS. Mainly for these reasons a detailed study is conducted considering the importance of changing curvature in the geometry of a hyperbolic paraboloid shaped TMS, and the process and results are presented in this chapter.

In structural mechanics, the process of form-finding is considered as an inverse problem, rather than a direct mechanism for estimation of forces and its consequences. In form-finding the equilibrium state of a structure is needed to be estimated on the basis of the imparted surface pre-stress and the applied boundary constraints/conditions. Past few remarkable studies (Dutta et al., 2016) suggest that the pre-stress is an important parameter to take care of in the TMS design process. For a future TMS structure , a designer specifies a target value of the pre-stress which is termed as the initial pre-stress value which is usually about 5-10% of the ultimate fabric tear strength. (Lewis, 2013)[Lewis, et al. 2003]. And this target pre-stress value is desired to be obtained in the end of the complete form-finding procedure for a TMS. This pre-stress is traditionally applied in the direction of the woven fabric yarns, i.e in the warp and weft direction. In other perspective it is applied parallel to the direction of doubly curved orientation of a TMS that are orthogonal to each other. It is also notable that initial pre-stress along the orthogonal directions can be equal or unequal in the magnitude, and this is the main reason for a wide range of structural forms obtained during the form-finding analysis of TMS (Topping, B H V, 2007). However, a study based on the minimal membrane surfaces containing the properties of consistent in-plane stress distribution throughout the surface gives the most stable form for any TMS subjected to a confined boundary conditions. The failure in terms of wrinkling, slackness and consequently pre-mature fatigue of the membrane material is prevented through this uniform stretching condition of a TMS surface (Lewis, 2013). Moreover, under the load application on this flexible

TMS, there are the chances of uniaxial tearing of fabric for a differently stressed (non-uniformly pre-stressed) surfaces due to a loss of pre-stress (Huntington, 2013).

4.2 Description and visualization of the Hypar TMS

The TMS considered for this work is a simple and real square hypar structure hinged supported in the corners. The plan, dimensions and elevation of the structure is displayed in the Figure 7 and Figure 8. This tensile membrane structure is taken from a round-robin exercise on the design and analysis of the membrane structures by Gosling et al., 2013. The main purpose of this analysis is to explore the scope of applicability of the stress reduction factors which are currently used for the designing of TMS along with the estimation of its consistency with the Eurocode 0. The finite element based simulation technique is applied to demonstrate a close to real behaviour of a TMS. This structure is one of the fundamental forms of a TMS and is very frequently utilized for membrane constructions. The description of the structure is given below:

1. The warp and fill directions are directed towards parallel to both the diagonals of the membrane yarn.
2. The initial pre-stress is oriented parallel to the warp and fill directions.
3. The warp and fill directions are in the orthogonal directions from the element local x and y axis respectively.
4. Material properties: Modulus of elasticity, E = 600.0 kN/m; Poisson's ratio, ν = 0.4; Yield stress, fy = 40.0 kN/m
5. Thickness of the membrane is 1 mm.
6. Geometry: $6m \times 6m$ square hypar, the opposite corner high points are H height above the two opposite low points.
7. Pre-stresses: Case I: warp = fill = 3 kN/m. Case II: warp = 5 kN/m; fill = 3 kN/m.
8. Edge cables: Cable diameter = 12mm, axial stiffness is equivalent to a Stainless Steel (Bar) A 479, Grade 316, 16Cr-12Ni-2Mo | ASME B31.3-2010. With elasticity modulus 205 GPa = 205 kN/mm^2.
9. Externally applied loadings: wind-uplift = 1.0 kN/m^2; snow load (ponding) = 0.6 kN/m^2.

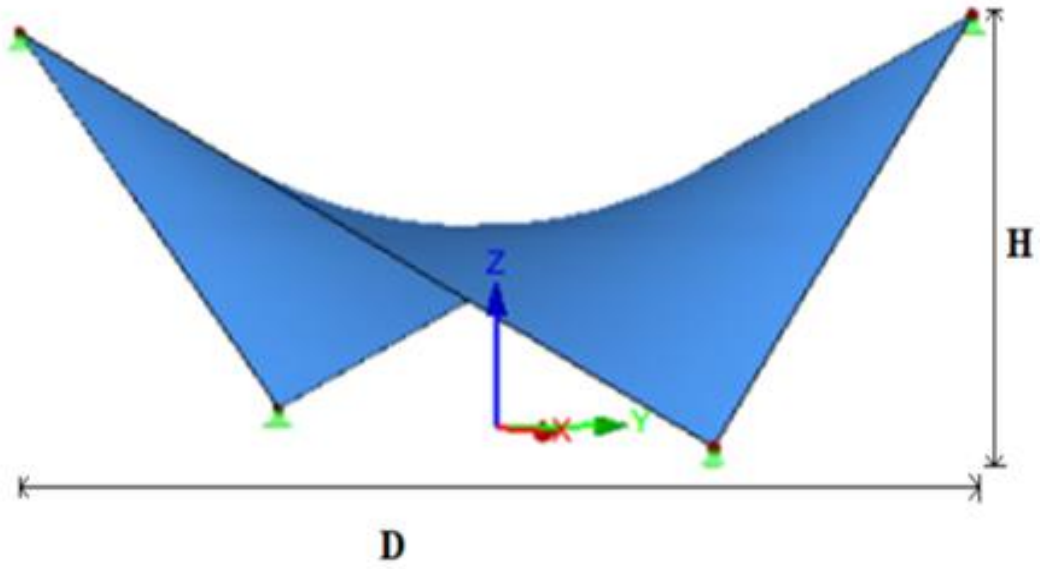

Figure 7 Isometric view of Hyparbolic Paraboloid TMS

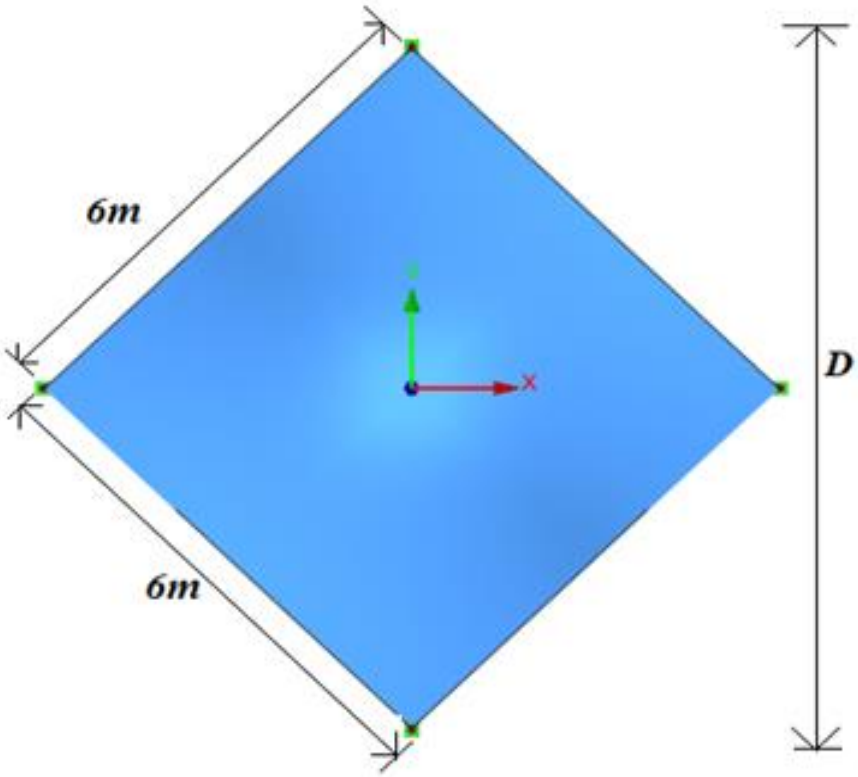

Figure 8 Plan view profile of the Hypar TMS

The TMS surface is meshed with the CST elements and the form-finding analysis begins with the initially defined surface topology. As the thickness of the fabric membranes used in the construction of TMS are negligible as compared to the other dimension,

consequently, the stresses along the thickness of the membrane are considered as negligible. Therefore it is important to point out that the stress values are expressed in kN/m, force per unit length of the membrane. The two different pre-stressing conditions isotropic pre-stress and anisotropic pre-stress are applied for the analysis. There are three DOFs per node (u_X, u_Y, u_Z) along the global X, Y, Z, coordinates. The edges of the structure are lined using the stainless steel cable. The supports are hinged with the boundary condition $u_X = 0, u_Y = 0, u_Z = 0$.

4.3 The Design Philosophy

Knowing the fact that, the surface pre-stress is responsible for carrying principal loads within the surface for a TMS with the help of a supporting structure, unlike steel, concrete or timber building elements which react to the external forces through bending. The Fabrics used in TMS possess negligible compression and bending stiffness, which indicates that the TMS must be designed with adequate curvature to contain the effect of environmental loads in resisting them through in-plane tensile and shear forces.

The shape and orientation of the TMS is vital to its ability to withstand the applied external loads predominantly in stressed form. To cope up with both the uplift forces and the downward forces, imparted mainly due to wind and snow respectively, the surface membrane must possess a doubly curved orientation and pre-stresses. To this extent it can be concluded that the detailed shape of a doubly curved surface structure is critical to its engineering and architectural performance. The curved geometry coupled with the initially induced pre-stress governs the distribution and magnitude of the stresses and the deformations subjected to applied load cases.

The equilibrium modelling is the most elementary base for the computational simulations implemented to examine the TMS design and analysis. The structure is discretized in small finite elements mesh with fixed topology, but with exception of fixed points, rather approximate nodal coordinates in local axis. Based on the type of finite element selection, the internal and external forces are determined and observed at the nodal points. Once external loads are applied, the out-of-balance forces at the nodes can be estimated. The residual force helps in the obtainment of the equivalent nodal points through the disturbed equilibrium state. The computational simulation approach for form finding is the efficient

way in prediction of member forces where both applied load and pre-stress is facilitated (Huntington, 2003).

The main focus of this study is to analyse the TMS behaviour in terms of deformation and the plane stresses under the influence of pre-stress and other loads. However, one grade of irregularity is also introduced to have a broader range of design possibilities. It is proven from a past case study of the Seoul South-western Baseball Stadium dome and the Jeju World Cup Stadium dome that the geometry of a TMS is the most influential factor (Kim et al., 2010)(Brzozowski et al., 2005). The geometry of a simple hypar shaped membrane structure can be easily moulded by changing the curvature observed between the two opposite high points of the membrane. Hence the curvature of the TMS is varied over a range between H = 1.5m to 3.5m, a detailed visualization of how the curvature is changing with height of the opposite high points is presented in the Figure 9.

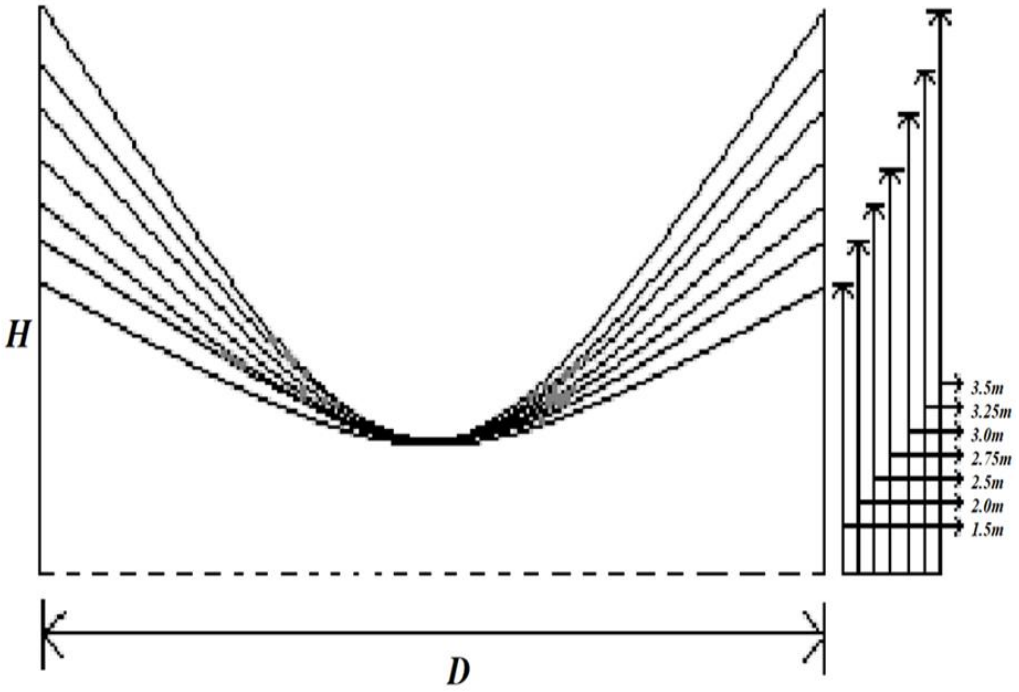

Figure 9 The height variation profiles of Hypar TMS

The external loads apart from pre-stresses are wind load and snow load and their combinations, the combination and classification of load cases considered for this study are implemented according to standard: ASCE 7-16 (minimum design loads and associated criteria for buildings and other structures), and the different load combinations are :

(a) Pre-stress
(b) Pre-stress + LC1(wind-uplift)
(c) Pre-stress + LC2(snow-load)
(d) Pre-stress + CO1(1.6*LC2)
(e) Pre-stress + CO2(0.5*LC1+1.6LC2)

After obtaining a form found hypar model, The loading conditions are implemented to carry out the stress deformation analysis for the structure. From the results, the two design based limitations are identified :- (a) the excess of the maximum allowed stress, which signifies that the model is not safe, and (b) the deformation avoiding the membrane clash with existing steel work or any other structural component.

4.4 Identification of the Limit State Functions

An allowable strength of 6.667kN/m is implemented, which is resembles a PVC coated polyester membrane with ultimate tensile fabic strength 40kN/m subjected to a stress reduction factor 6. The consideration of load cases and combination is implemented according to ASCE 7-16 (minimum design loads and associated criteria for buildings and other structures).

The limit state for this structure can be defined as:

- Limiting warp stress : $G_1 = \sigma_{permissible} - \sigma^{w}_{max.}$
- The Wrinkling criteria: $G_2 = \sigma^{P}_{\min imum} - \sigma^{P}_{permissible}$
- Deflection criteria: $G_3 = D_{allowable} - D_{Maximum}$

The allowable deflection for the study is arbitrarily chosen as L/60, i.e. 100mm, due to lack of proper guidelines the main reason for such a limit state for deflection is mainly centred to address the issues like, overlapping of membrane with supporting steel work and ponding due to precipitation. $\sigma_{permissible}$ is calculated as,$\sigma_{permissible} = \sigma_{ultimate}/6$ and $\sigma^{p}_{permissible} = 0$, based on the stress states presented in table no. 1. For this study the random variables considered are supposed to be normally distributed and a standard deviation of 10% (COV = 0.10) of the mean value for each variable is set initially.

In this TMS example the probability of failure of a pre-stressed hyperbolic paraboloid made up of poly vinly chloride coated fabric membrane is considered. A combination of both probabilistic (statistically defined) and deterministic parameter is implemented. The selection of the values of a statistical parameter is decided based on the available statistical information.

4.5 Results and Discussions

The hypar TMS responses to the prescribed loads and loading combinations are obtained in terms of deformation and stresses (warp/fill). The direction for accounting deformation is taken as z-axis, the reason for choosing z-axis is that, the wind and snow forces are acting parallel to this direction. The results here are described in two stages, first the deformation and warp-fill stresses results are presented in the form of stress-deformation analysis and form-finding procedure. The results of reliability indices corresponding to subjected limit states are examined in the second part of the results.

4.5.1 Form-finding analysis bound for different height of hypar shaped TMS in the isotropic pre-stressing scenario

The applications of isotropic pre-stress have resulted in linear variation of the maximum deformation of membrane surface. This implies that the maximum allowable deflection will fall under the deflection limit state of 100mm when an isotropic pre-stress is applied under the prescribed loading environment. The variation profile for this load case is found to be coinciding with the deformation trend line with positive gradient.

Figure 10 represents the initial simulations which were designed for the seven different curvatures, and the final shapes were obtained from the form-finding procedure. The initial stress distribution in the elements of the warp and fill sections after the form-finding analysis can be read from Table 6. The distribution of the initial stresses should be intend to balance both warp and fill directions and along each and every finite element.

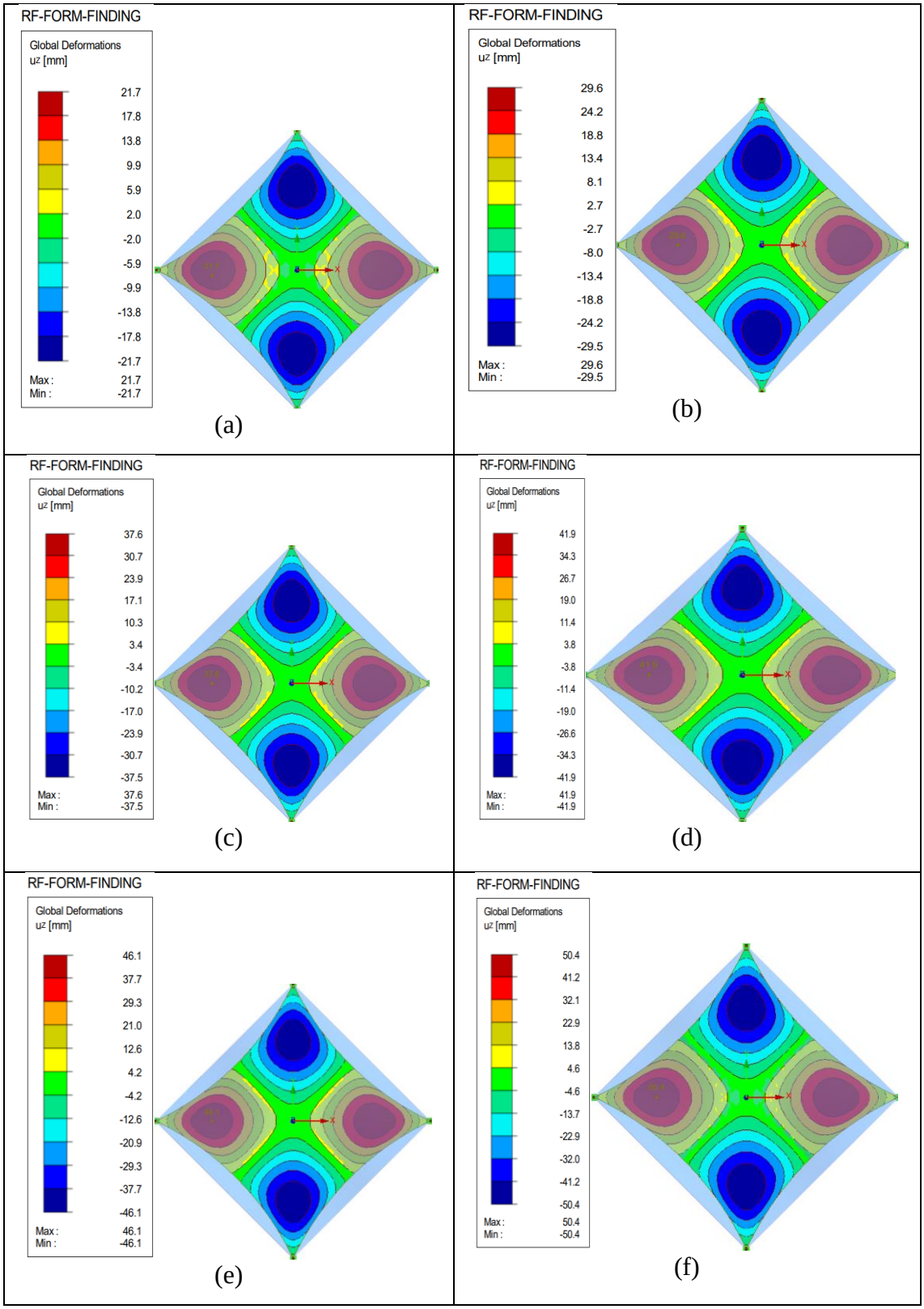

Figure 10 The form-found simulation models displaying maximum deformation contours for Isotropic pre-stressing of Hypar TMS

A non-linear finite element analysis of the TMS gives a maximum warp stress of 3.63kN/m and maximum stress in fill direction as 3.14 kN/m. The maximum deformation for form-finding analysis happened for the case of maximum warp and fill stresses. The

TMS structural response in terms of deformation and stresses with maximum magnitude has happened for the TMS height case 3.50m. The maximum deformation of 54.82mm is observed during the analysis, which is under the range of the deflection limit of 100mm as allowable deformation adopted for the present study.

Table 6 Description of deformation and stresses for form-finding of Hypar TMS

Height in m.	**1.50**	**2.00**	**2.50**	**2.75**	**3.00**	**3.25**	**3.50**
Warp stress, n_x (kN/m)	3.13	3.27	3.34	3.41	3.48	3.55	3.63
Fill stress ,n_y(kN/m)	3.08	3.14	3.22	3.27	3.32	3.37	3.41
Deformation along z-axis (mm)	21.71	29.63	37.65	41.94	46.12	50.44	54.82

The magnitude of maximum warp stresses and minimum fill stresses obtained during the form-finding analysis are mentioned in Table 6. The warp and fill stress distribution contours for TMS height case 3.5m are displayed in Figure 11(a), (b).

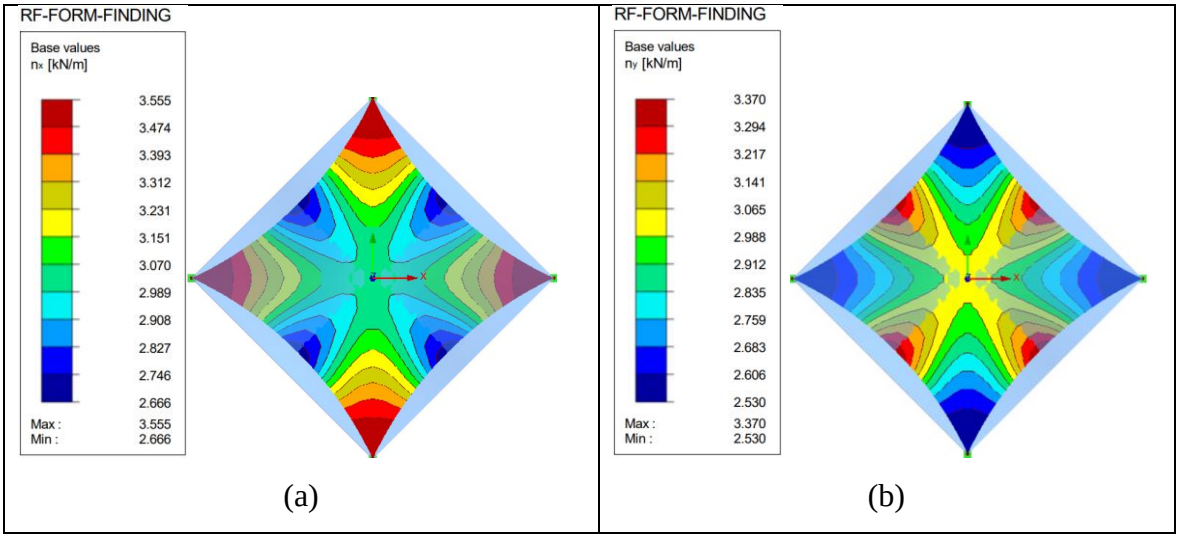

(a) (b)

Figure 11 warp stress contours (a) and fill/weft stress contours (b) for height 3.5m of Hypar TMS

4.5.2 Form-finding analysis bound for different height of hypar shaped TMS in the Anisotropic pre-stressing scenario

The results of deformation for form-finding procedure are seems to be increasing gradually with increase in the height of the structure, with a slight depression in the deformation curve for height case 2.5 m Figure 12. The deformation for all the cases are

observed to be more than the limiting value i.e. 100mm, varying from 114.2mm to 235.0 mm. This highlights that in case of anisotropic pre-stressed hypar TMS, the deformation limit state for design should be considered only for the serviceability requirement.

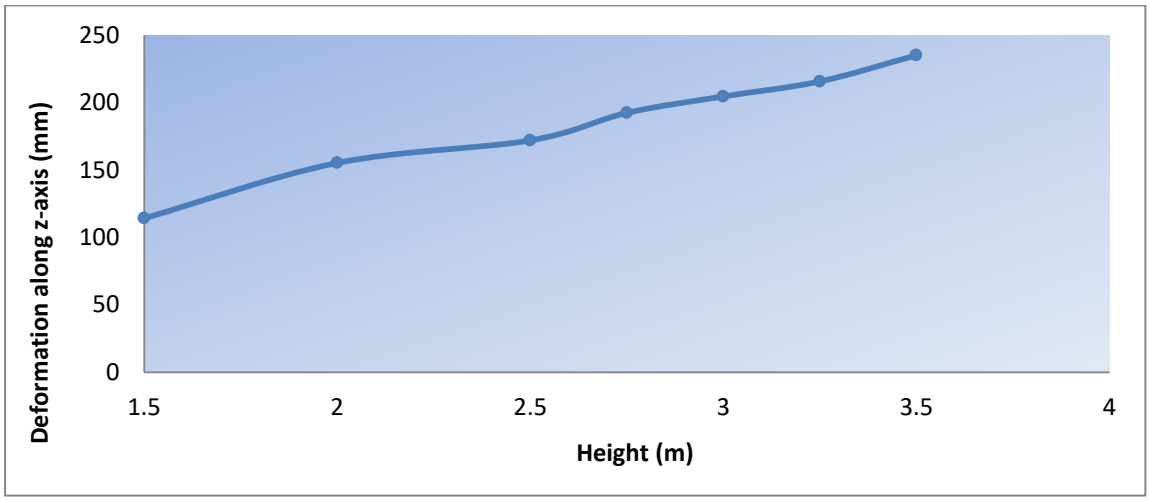

Figure 12 Deformation along z-axis for form-finding of Hypar TMS (anisotropic)

The simulation models for form-finding analysis were generated for each height of the structure. The Figure 13 below display the deformation contours and highlighting the maximum and minimum deformation region. According to the contours, the region near corners seems to experience maximum deformations.

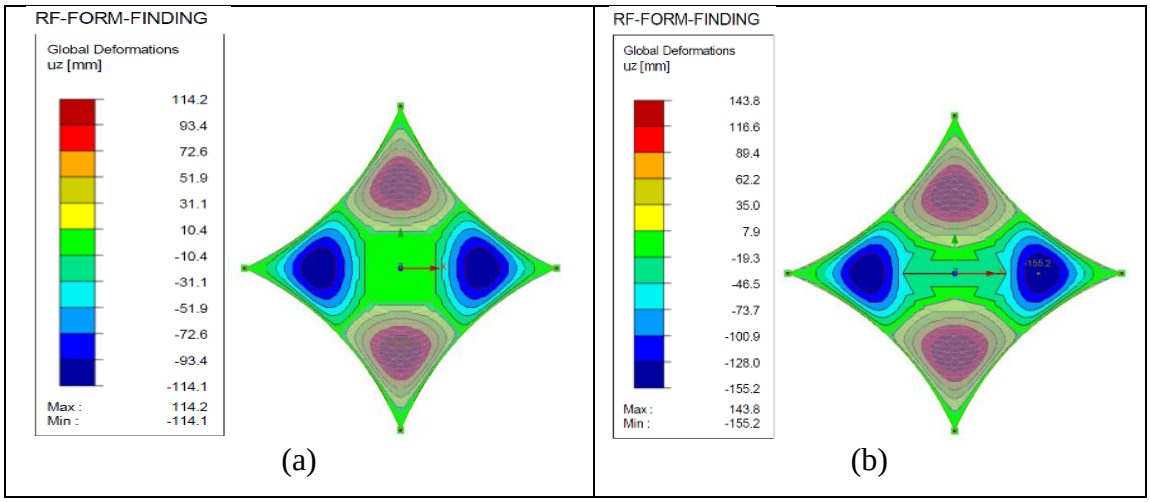

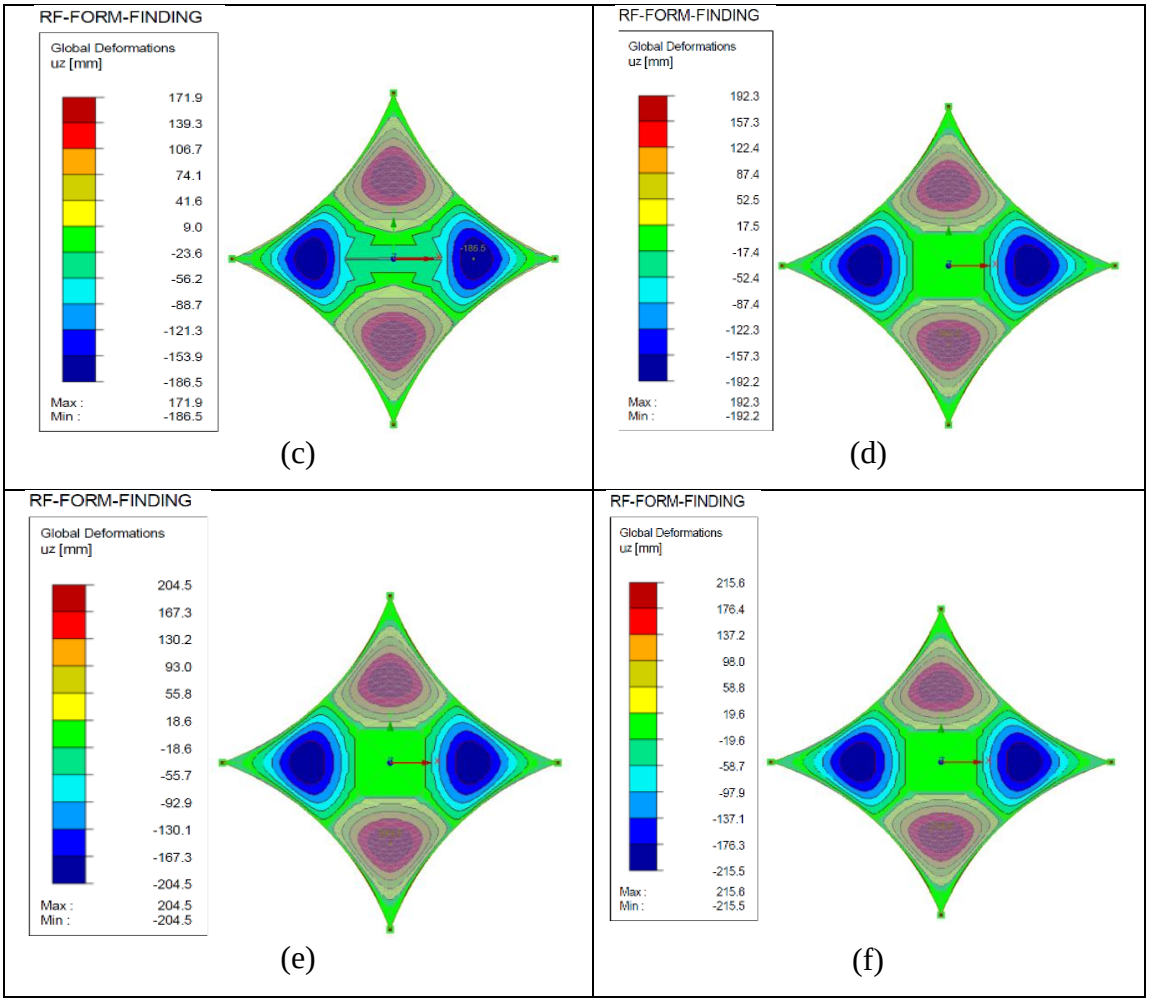

Figure 13 Deformation contour models of anisotropic pre-stressing of Hypar TMS

The maximum warp stress and minimum fill stress for each cases after form-finding analysis are recorded in the Table 7 below. In response to the initially imparted stress of 5 kN/m in warp direction and 3 kN/m in fill direction for each structure, we have received the maximum warp stress of 6.16 kN/m for the structure with height 2.75m, the fill stress have attained a uniform stresses of around 2.96 kN/m for almost each case of TMS with different height as can be observed from the Table 7.

Table 7 The description of deformation and stresses as an outcome of form-finding procedure for anisotropic pre-stressing of Hypar TMS.

Height in m.	**1.50**	**2.00**	**2.50**	**2.75**	**3.00**	**3.25**	**3.50**
Warp stress, n_x (kN/m)	6.14	5.63	5.63	6.16	6.15	6.15	5.65
Fill stress ,n_y(kN/m)	2.97	2.96	2.96	2.96	2.96	2.96	2.95
Deformation along z-axis (mm)	114.2	155.2	171.9	192.3	204.5	215.6	235

The stress distribution contours suggesting the regions of maximum and minimum level of pre-stressing experienced after form-finding analysis are displayed in the Figure 14. Looking into the legends in the picture, for TMS height case 3.5 m the warp stress have varied from 3.53 kN/m to 5.657 kN/m and the fill stress have fluctuated between 2.96 kN/m to 3.63 kN/m.

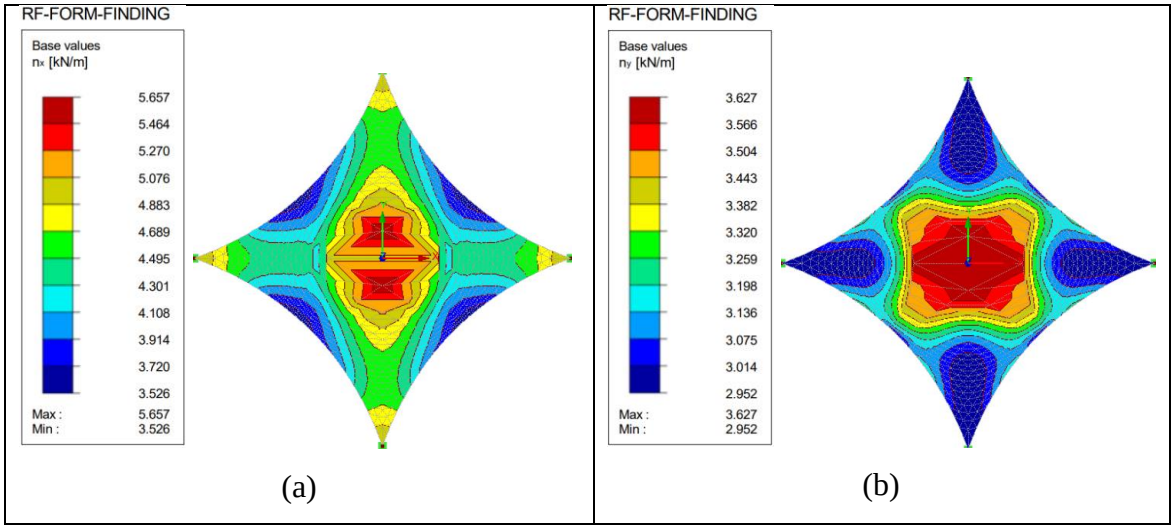

Figure 14 The warp stress (a) and fill stress (b) distribution contours for form-finding process of anisotropic pre-stressing of Hypar TMS**.**

4.5.3 Stress-deformation analysis for various loads and load combinations for isotropic pre-stress Hypar TMS.

After attaining the perfect shapes for an isotropically pre-stressed hypar shaped TMS from the form-finding analysis, the stress-deformation analysis is executed for various loading conditions both downwards and upwards loadings. The load combinations for the analysis are incorporated as per ASCE 7-16 national annex (Minimum Design Loads and Associated Criteria for Buildings and Other Structures). As premeditated earlier that, if the initial stressing of TMS surface is not balanced after the form-finding process, the structure might have an erratic behavior. A poor form-finding of the surface will induce the possibilities of breaching maximum allowable stresses, zero stress regions or zero permissible stress development (wrinkling) after the stress deformation analysis.

It is for that reason; the stress-deformation investigation is must to evaluate the overall performance of these models in order to achieve a clear conclusion. The results of maximum warp stresses (along x-axis) and minimum fill/weft stresses (along y-axis) for the various loads and load combinations are tabulated in Table 8 and Table 9**.**

Table 8 The maximum warp stress responses for various load cases and different height for isotropic pre-stressing of Hypar TMS

Load cases as per ASCE 7-16	**Maximum warp stress kN/m for variation of height H**						
	1.5 m	2.0m	2.5m	2.75m	3.0m	3.25m	3.5m
Pre-stress	3.13	3.27	3.34	3.41	3.48	3.55	3.63
LC1(wind-uplift)	3.69	3.83	3.97	4.05	4.12	4.20	4.29
LC2(snow-load)	3.42	3.55	3.70	3.78	3.86	3.94	4.03
CO1(1.6*LC2)	3.66	3.80	3.94	4.02	4.10	4.18	4.26
CO2(0.5*LC1+1.6LC2)	3.34	3.46	3.61	3.68	3.76	3.84	3.93

The variation of maximum warping stresses suggest that the membrane surface will keep on stretching and will result in the development of uniform strain for all the load cases considered in this study. The load cases wind uplift and heavy snow load are prone to develop maximum warp stresses. The results shows that the maximum of the maximum stress which is 4.29 kN/m corresponding to H=3.5m for wind-uplift load case, is falling under the range of permissible limit stress of 6.67 kN/m even after implementation of stress reduction factor. This indicates a safe design possibility of a Hypar TMS under given loading environment.

Table 9 The minimum fill/weft stress responses for various load cases and different height for isotropic pre-stressing of Hypar TMS

Load cases as per ASCE 7-16	**Minimum fill stress kN/m for variation of height H**						
	1.5 m	2.0m	2.5m	2.75m	3.0m	3.25m	3.5m
Pre-stress	2.87	2.79	2.69	2.63	2.58	2.53	2.47
LC1(wind-uplift)	2.69	2.68	2.61	2.58	2.55	2.52	2.47
LC2(snow-load)	2.86	2.78	2.62	2.61	2.5	2.49	2.43
CO1(1.6*LC2)	2.73	2.69	2.63	2.59	2.56	2.52	2.46
CO2(0.5*LC1+1.6LC2)	2.87	2.77	2.67	2.61	2.55	2.49	2.44

The results of fill or weft direction stresses suggests that there is a continuous decrement in the fill direction stresses for all the load cases. The minimum of the minimum fill stresses obtained is around 2.4 kN/m for almost all the load cases and this minimum fill stress is observed for the height 3.5m. The minimum permissible stress for containing the design under the wrinkling limit state is zero. Hence the results of the analysis indicates an acceptable design methodology with respect to the minimum permissible stress criteria. The development and variation of stress contours for all the load cases for height case H = 3.5m are demonstrated in the Figure 15 below. The stress contours for form finding process are shown previously in section 4.2.1.

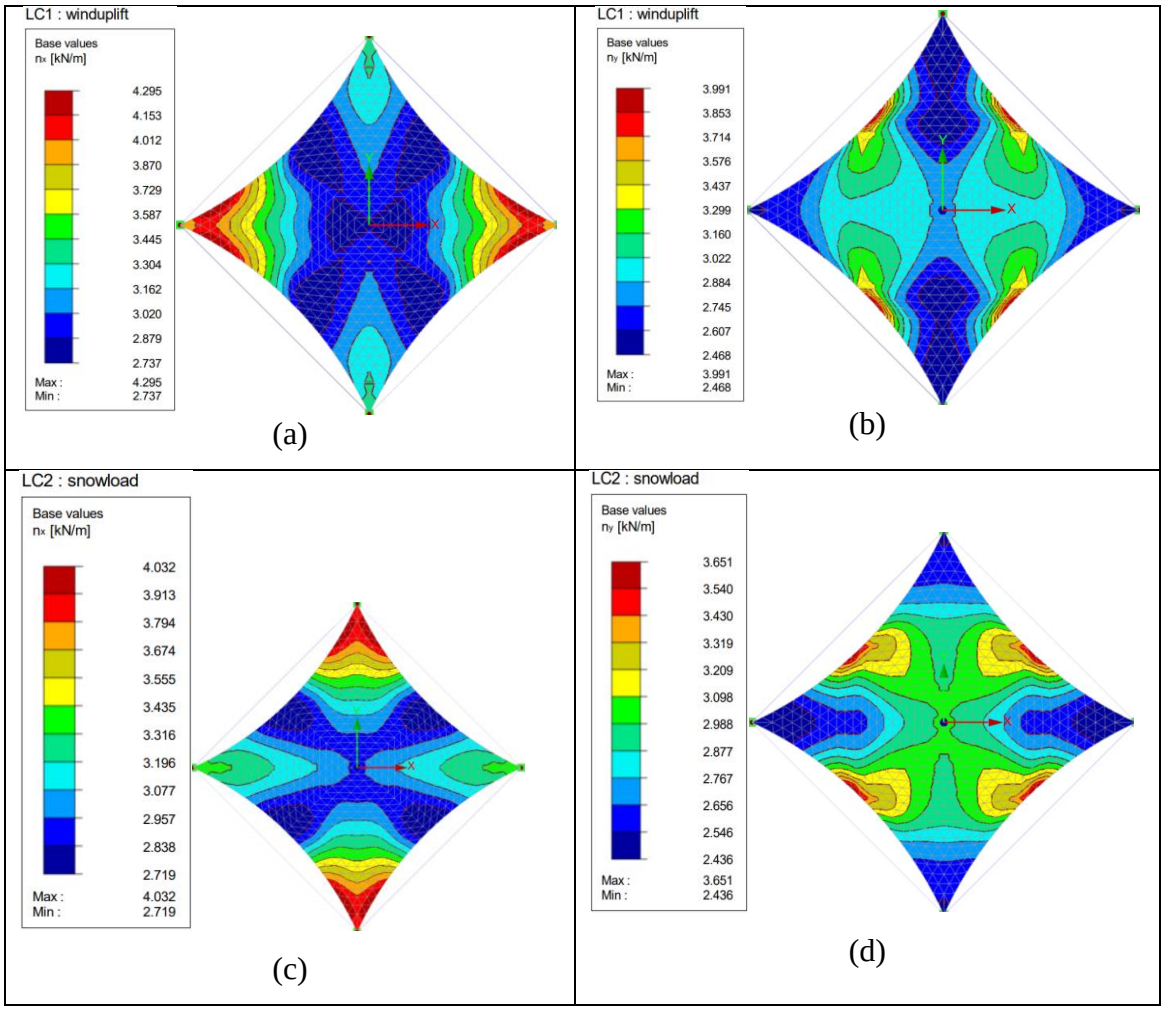

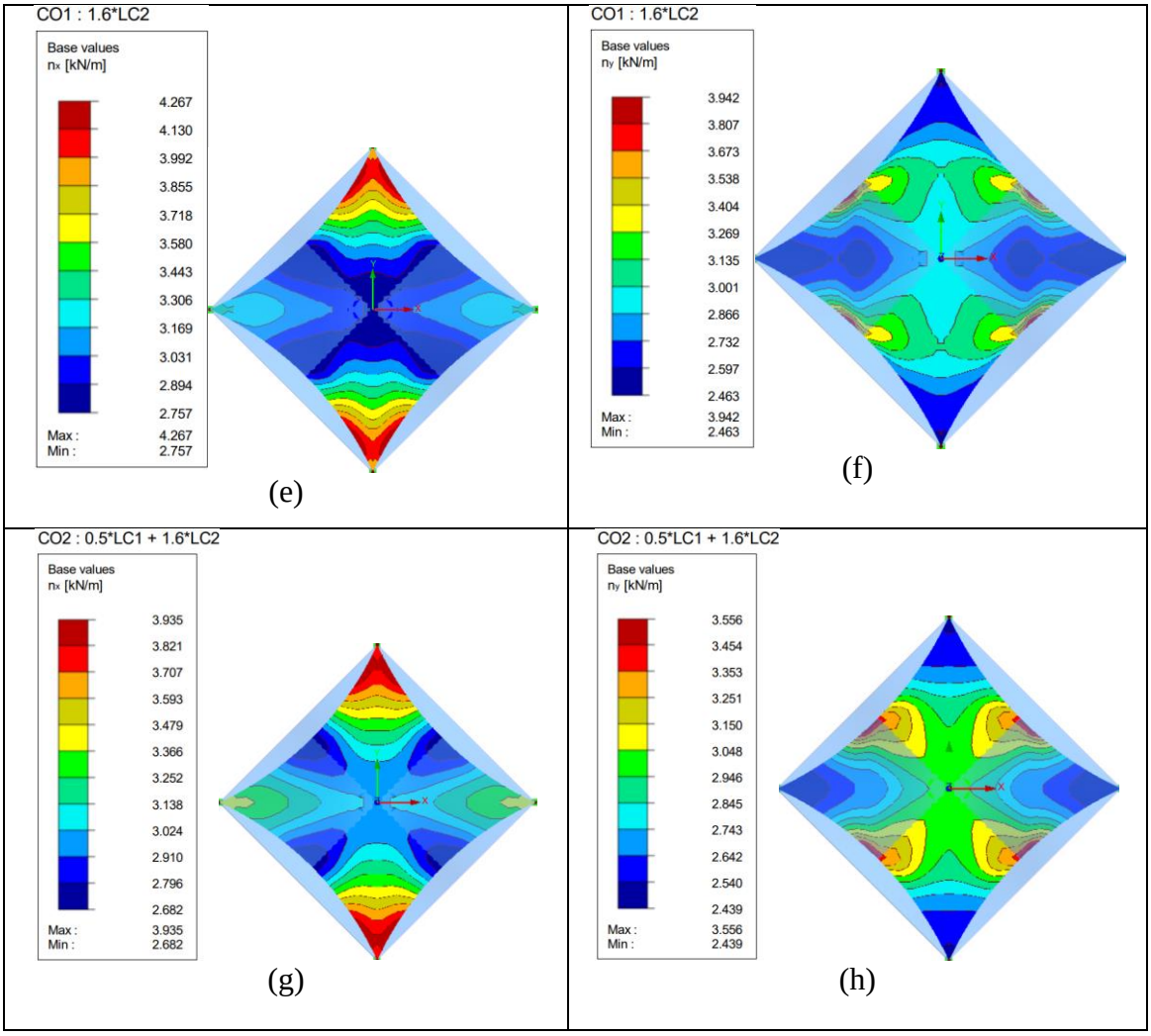

Figure 15 The warp and fill stresses development contours after stress-deformation analysis for isotropic pre-stressing of Hypar TMS

The major information which can be obtained from the simulation models for stress distribution is that, in case of warp stress the maximum magnitude is experienced around the corner aligned parallel to the weft direction. And in the case of fill stress the maximum magnitude is observed along the edges at the region around mid-point of the span. This shows a very good agreement with the findings of a latest research (Rana B.,S. et. al., 2022) which highlights the fact that the middle of the edge span length of corner supported TMS is more sensitive to the point load applied along with the pre-stressing. In this case it is the uniformly distributed load which shows maximum strain in the edge mid-span region.

4.5.3.1 Maximum deformation of TMS due to change in the coefficient of curvature for Isotropic pre-stressing of hypar shaped TMS.

The details of deformations for the form-finding case is discussed in the previous section 4.5.1, the deformations due to other load cases are tabulated in the Table 10 below. It can be seen that *LC1* (wind-uplift) evidences the maximum deformation which is even more than 1.0 m for height 1.5m. Such kind of deformations makes no sense in the conventional structural analysis. The load case *CO1(*1.6 times snow load) also shows deformations closer to 1.0 m, with a decreasing trend and evidences minimum deformation of 565.1mm for the height case 3.5m.

Table 10 The z-axis maximum deformations for each load case corresponding to height variation of Hypar TMS

Load cases as per	**Variation of the height (H) in m.**						
ASCE 7-16	**1.5**	**2.0**	**2.5**	**2.75**	**3.0**	**3.25**	**3.5**
Pre-stress	21.7	29.6	37.6	41.9	46.1	50.4	54.8
LC1(wind-uplift)	1071.1	1053.8	1033.2	1023.7	1014.4	1005	996.8
LC2(snow-load)	546.2	549.2	552.9	554.7	557.4	560.3	565.1
CO1(1.6*LC2)	998.2	986.5	971.7	965.1	958.7	952.3	498.5
CO2(0.5*LC1+1.6LC 2)	408.7	412.4	416.7	419.2	421.3	425.0	429.7

A better visualization of the regions of deformations for each height case in the scenario of each type of loading is discussed in the next section of the chapter.

4.5.3.2 The demonstration of deformation contours for Hypar TMS (Isotropic Pre-stress)

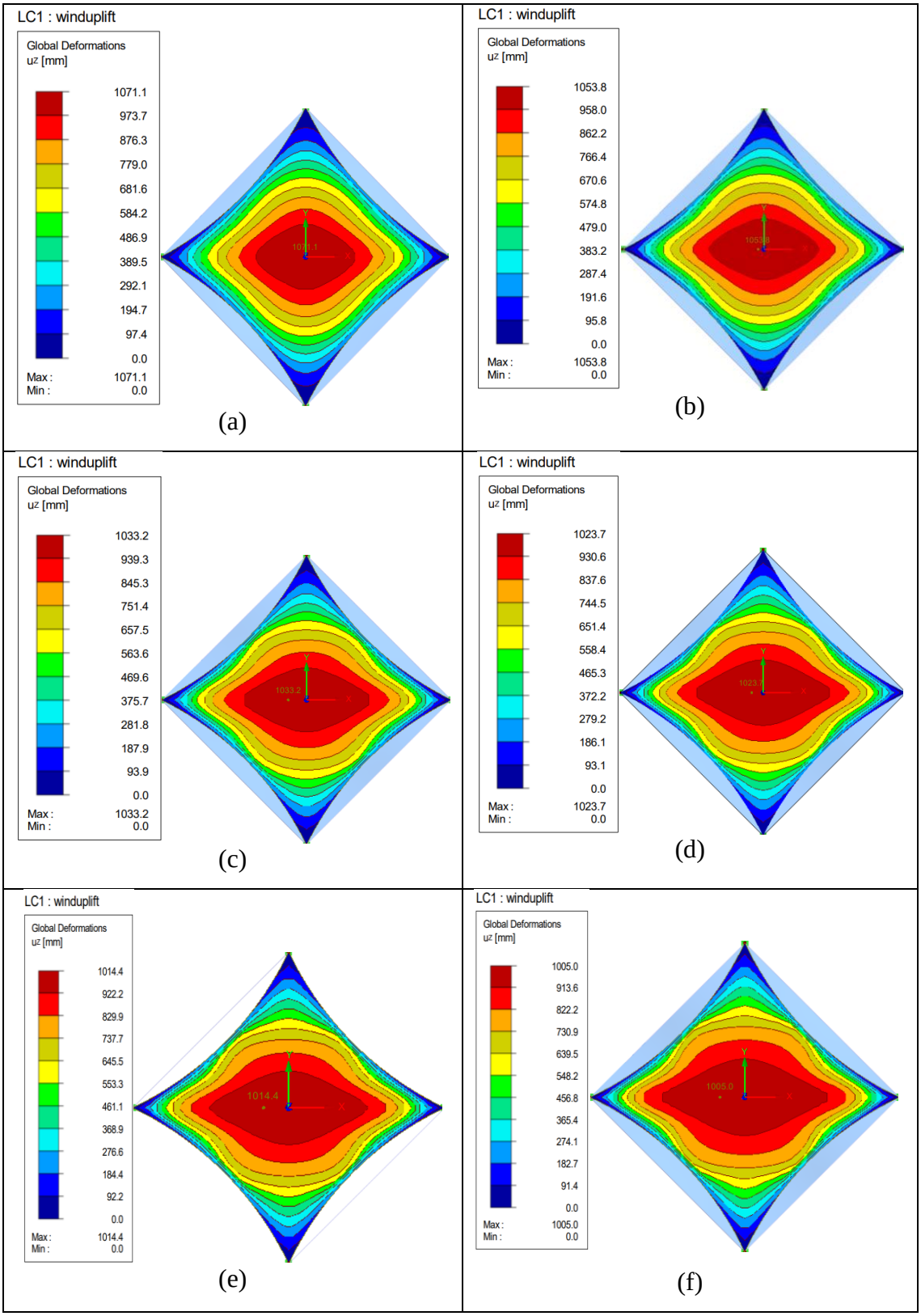

Figure 16 The deformation contour models for wind-uplift load case of Hypar TMS (isotropic pre-stress)

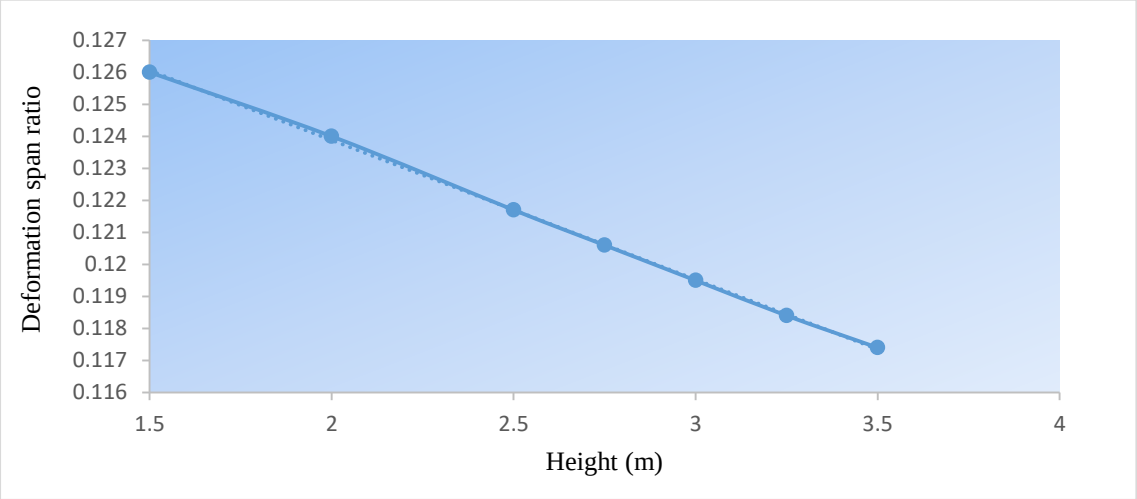

Figure 17 The deformation span ratio under wind-uplift for deflection along z-axis for Hypar TMS (Isotropic pre-stress)

The variation of maximum deformation along z-axis with the application of wind-uplift of 1.0 kN/m^2, obtains very high deformation scenario subjected to the present loading and supporting conditions**.** A maximum deformation span ratio of 0.126 is obtained for the hypar TMS of height 1.5m. The development of warp and fill stress subjected to current loading and height may give a better assessment of the failure situation and the sudden drop of deformation from H= 2.5 m to 2.75 m.

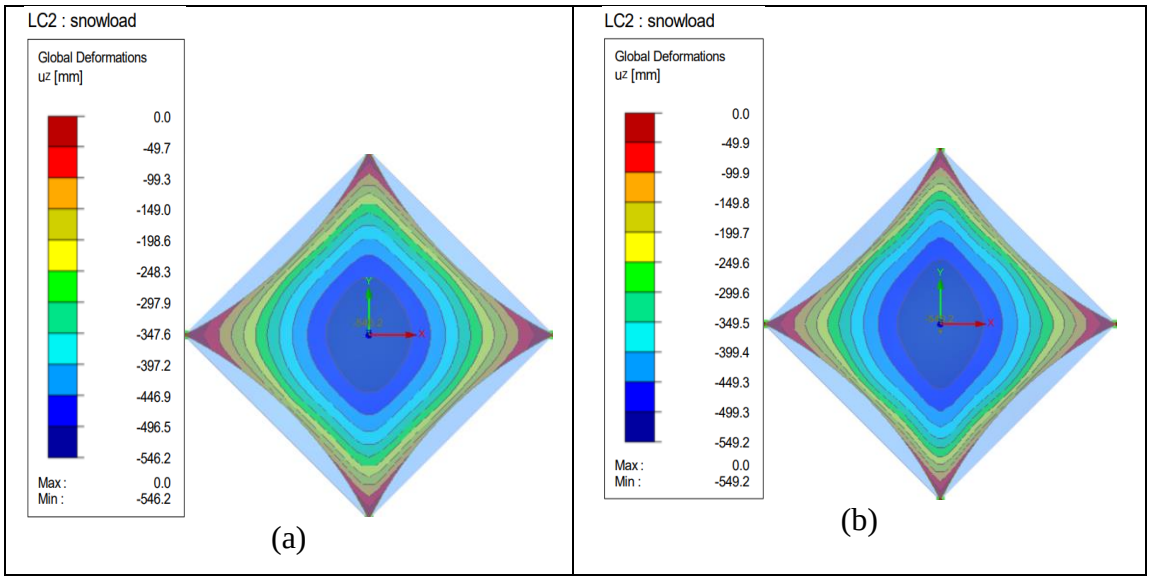

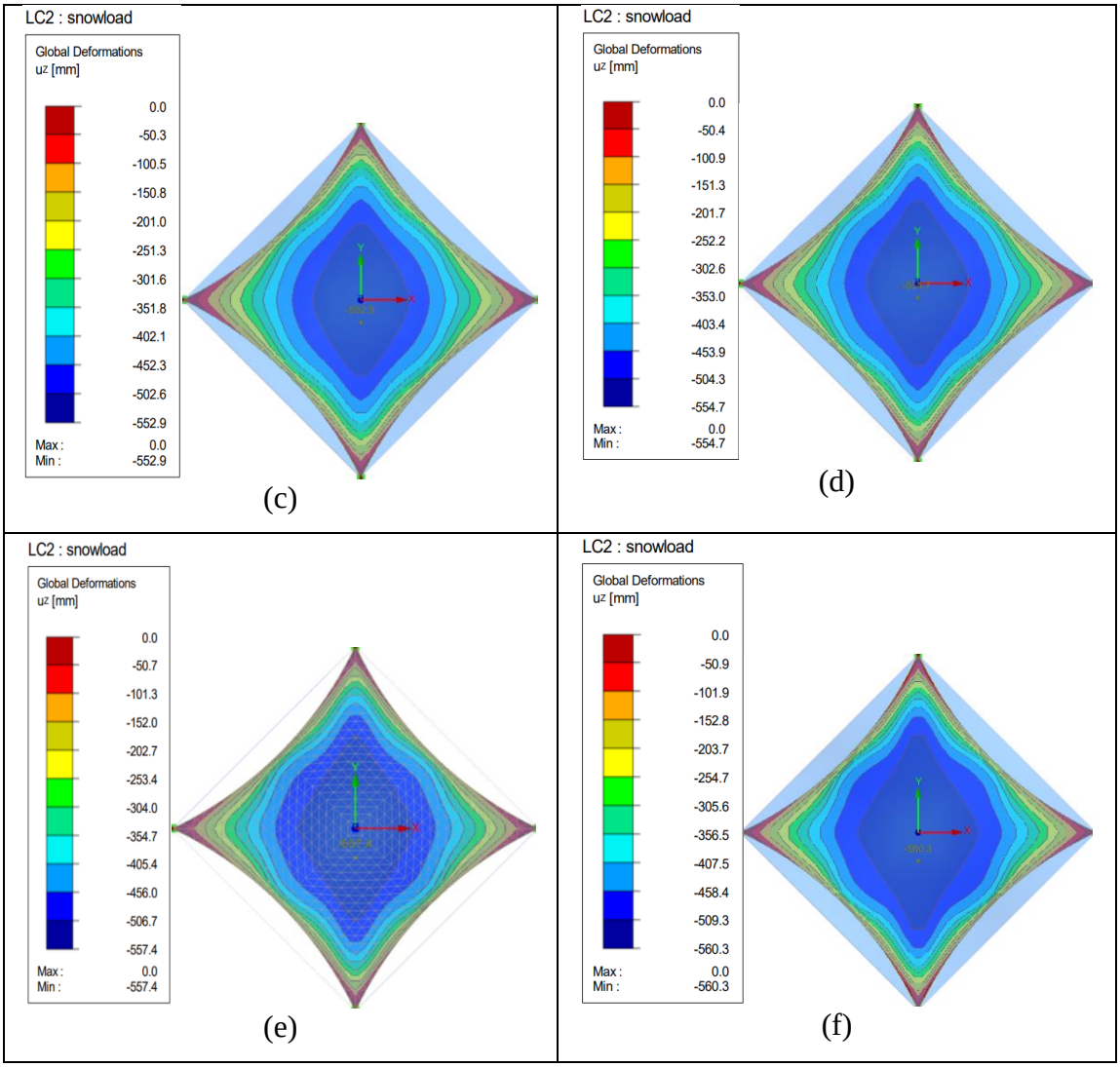

Figure 18 The deformation contour models for snow load case of Hypar TMS (isotropic pre-stress)

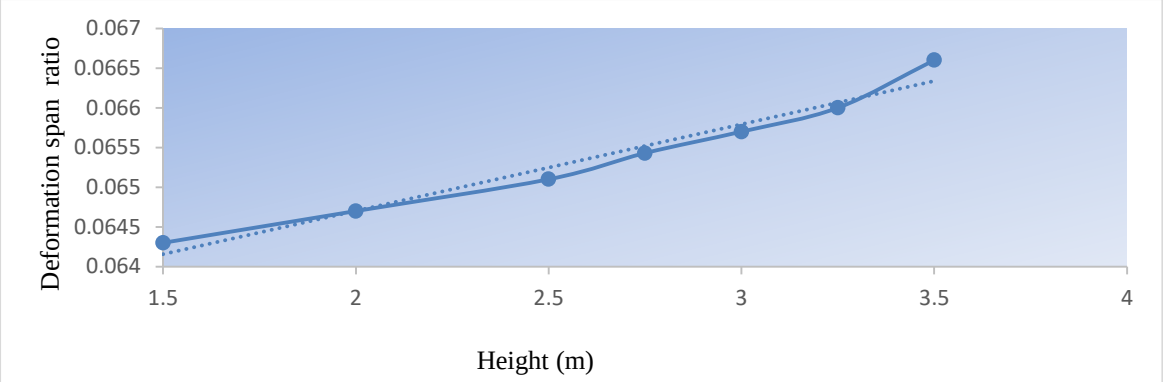

Figure 19 The deformation span ratio under snow-load for deflection along z-axis for Hypar TMS (Isotropic pre-stress)

The deformation caused by snow ponding for a snow load of 0.6kN/m^2 acting vertically downward direction follows a uniformly progressive pattern with a maximum deflection range variation of approximately 20 mm for the change in height from H= 1.5 m to 3.5 m. Although the deflection behaviour in this case is changing uniformly with the height, it is still far away from the range of allowable deformation of 100 mm considered for the deflection limit state.

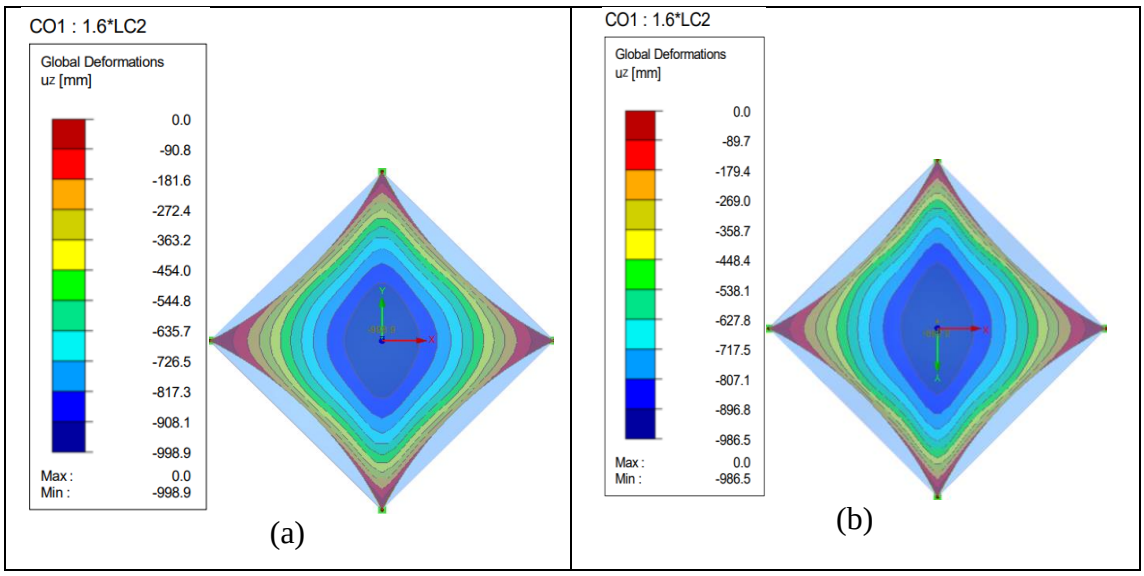

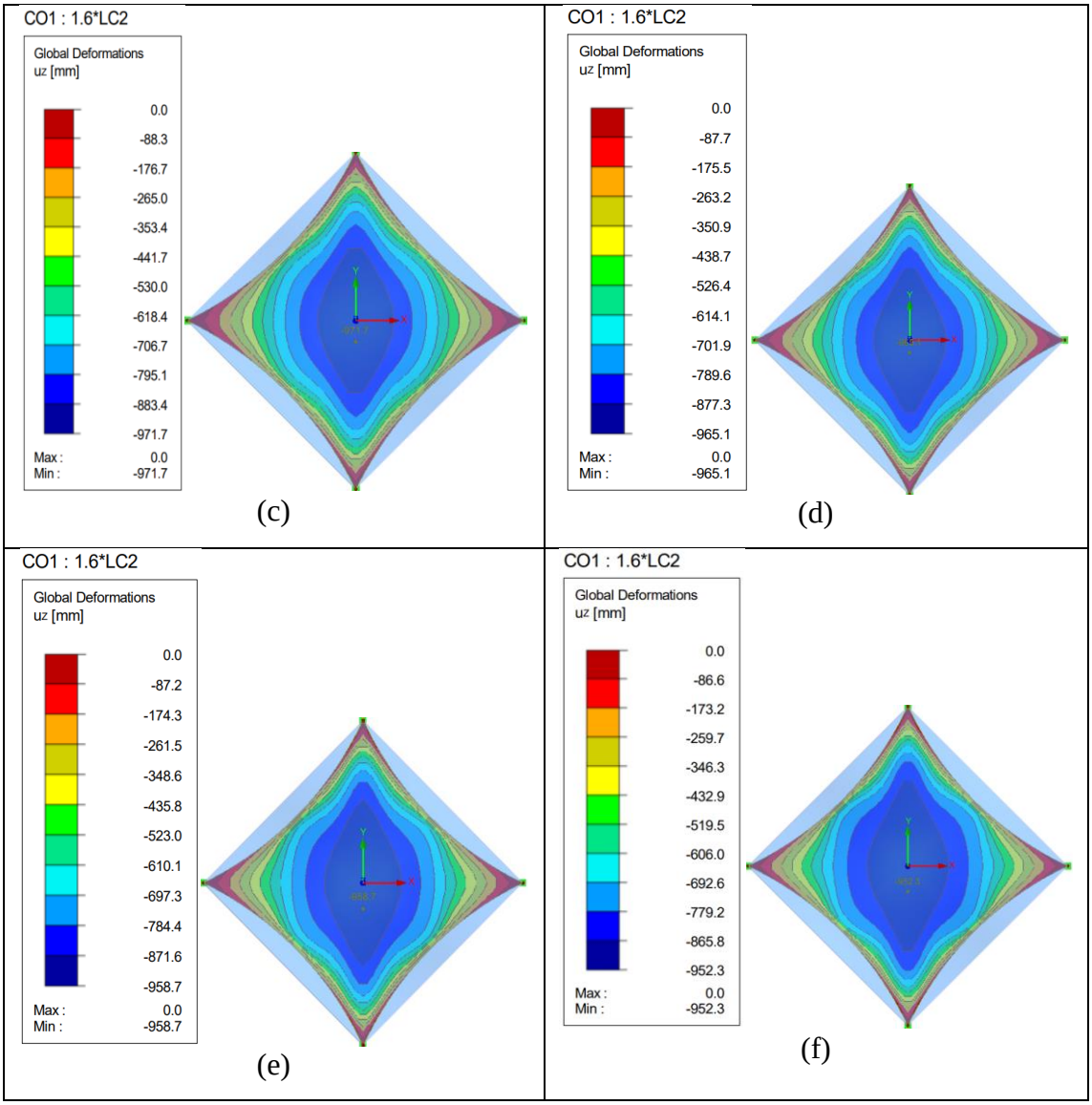

Figure 20 The deformation contour models for CO1 load case of Hypar TMS (isotropic pre-stress)

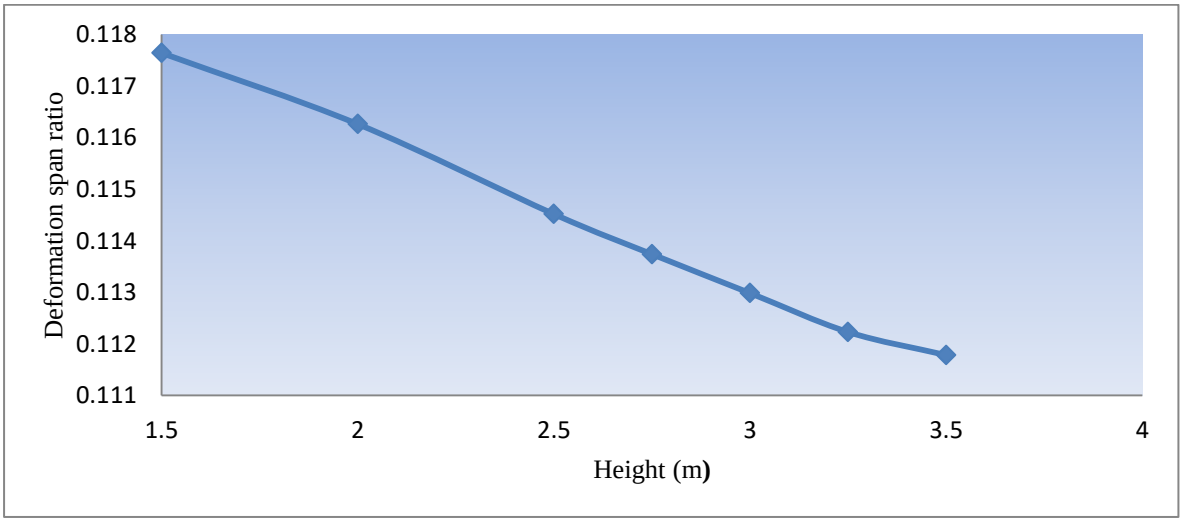

Figure 21 The deformation span ratio under CO1(1.6*snow-load) for deflection along z-axis for Hypar TMS (Isotropic pre-stress)

The load case *CO1(1.6*snowload)* may be interpreted as the condition of relatively heavy snowfall. The maximum deformation profile for this load case follows a trend line with negative gradient, meaning that the deformation in this type of load case can be governed by controlling the height and warp direction curvature of a Hypar TMS. The closer assessment of the warp and weft stresses developed can give a better understanding of the sudden drop of maximum deformation with change in height from H= 3.25m to 3.50m.

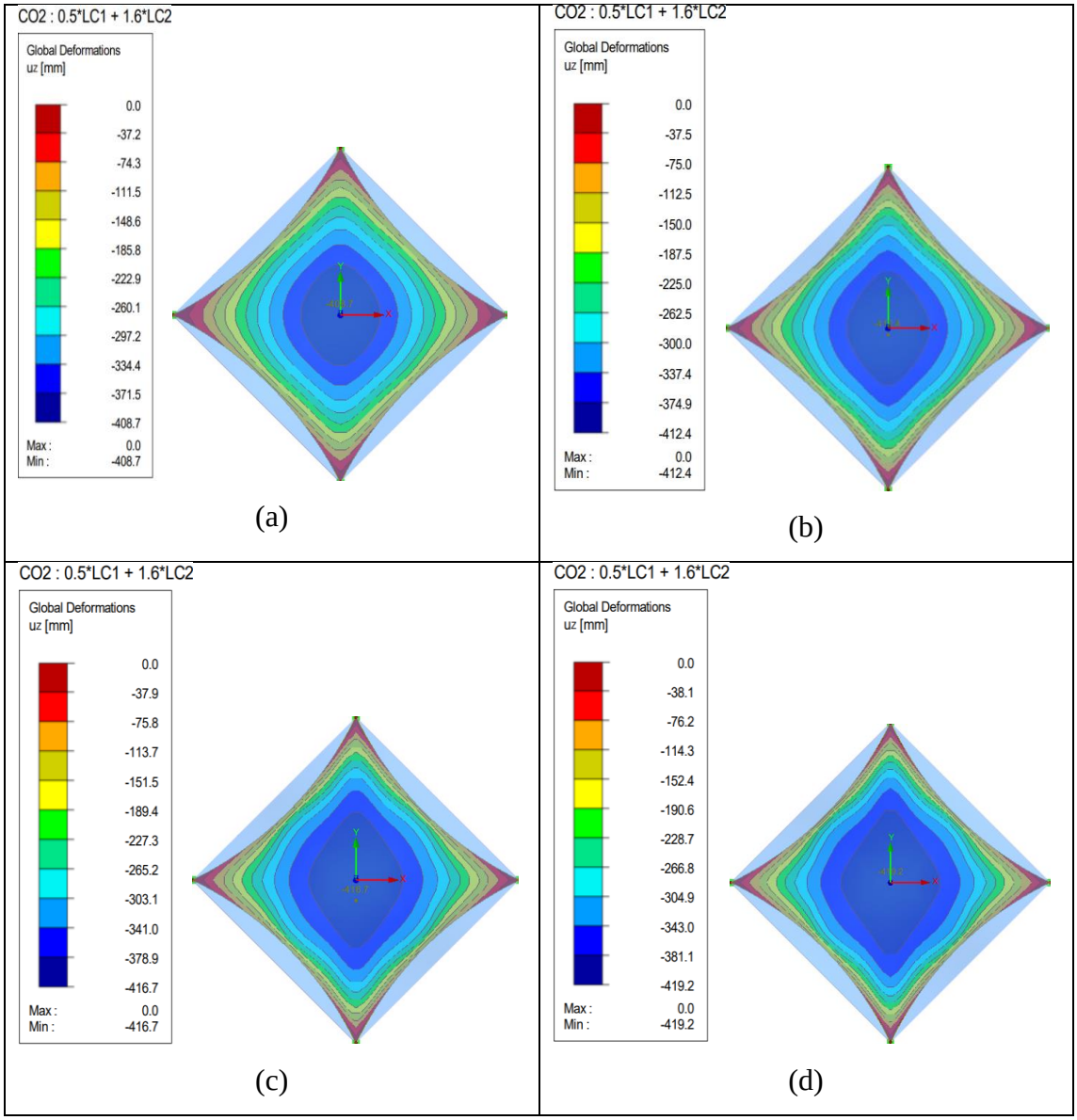

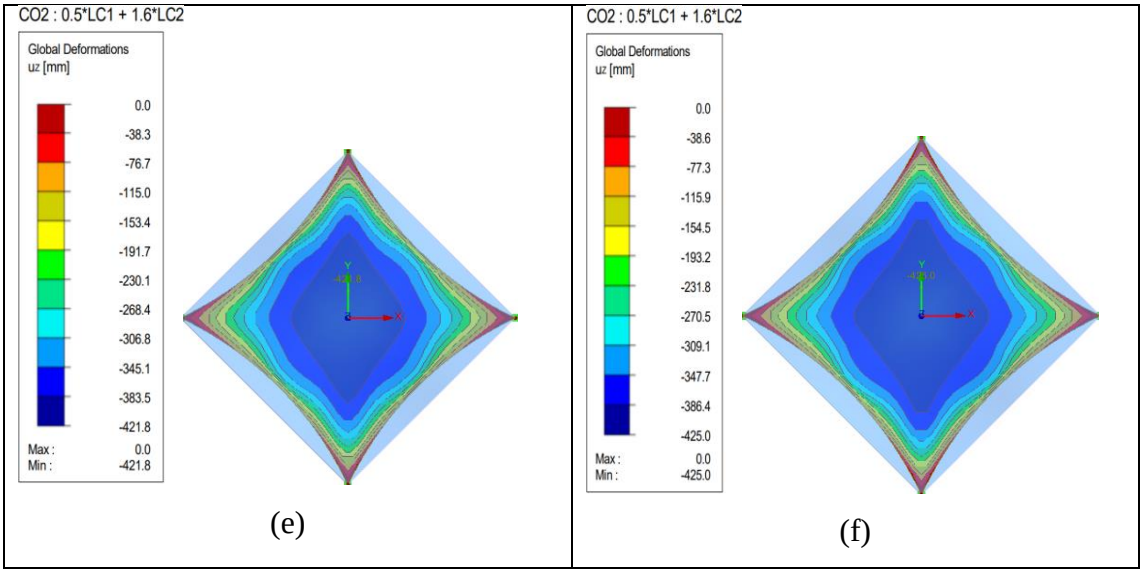

Figure 22 The deformation contour models for CO2 load case of Hypar TMS (isotropic pre-stress)

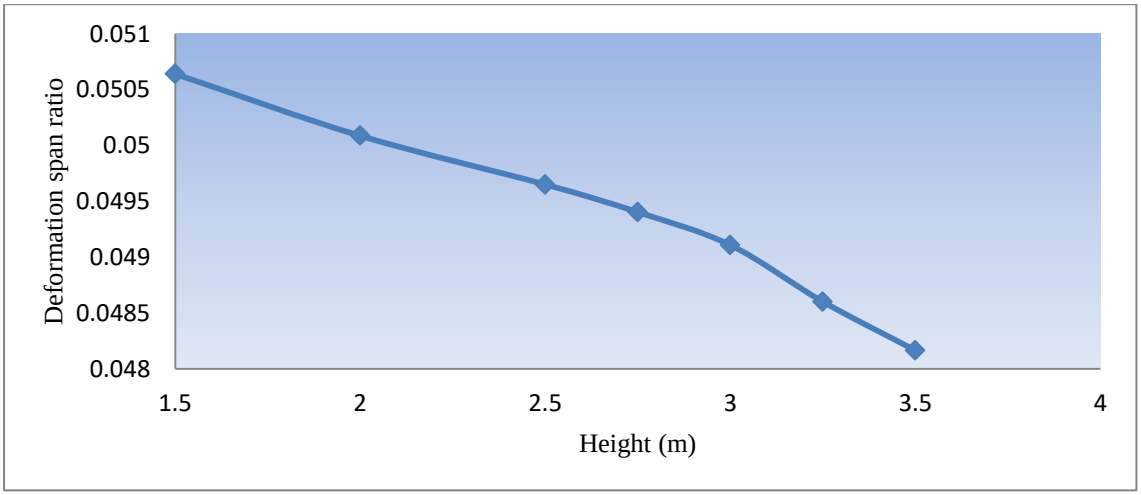

Figure 23 The deformation span ratio under *CO2(0.5*wind-uplift +1.6snow load)*for deflection along z-axis for Hypar TMS (Isotropic pre-stress)

This type of load case may manifest the situation of heavy precipitation along with moderate wind conditions. The deformation profile suggests that a progressive maximum deformation will be obtained in this case, the reason for relatively low deformation as compared to load cases: - wind uplift, snowfall and heavy snowfall is mainly because the snow load and wind uplift force are acting in the opposite directions.

4.5.4 Stress-deformation analysis for various loads and load combinations for Anisotropic pre-stress Hypar TMS.

On applying 5.0kN/m of pre-stress in warp direction and 3.0kN/m of pre-stress in fill direction, the results of stress-deformation analysis of hypar membrane shows interesting pattern unlike isotropically pre-stressed membrane. Warp stresses are observed to be fluctuating considerably while varying the height of the structure. From Table 11 it can be seen that the maximum warp stresses are over 6.0 kN/m for heights 1.5m, 2.75m, 3.0m and 3.25m. While on the other hand the maximum warp stresses are recorded to be falling around 5.5kN/m of magnitude for 2.0m, 2.5m, and 3.5m. Hence it is evident from the results that in order to acquire minimal surface area orientation, the prescribed hypar TMS should be constructed with the height 2.0m, 2.5m or 3.5m.

Table 11 The maximum warp stress description of stress-deformation analysis of Hypar TMS (anisotropic stress)

Load cases as per ASCE 7-16	**Maximum warp stress kN/m for variation of height H**						
	1.5 m	**2.0m**	**2.5m**	**2.75m**	**3.0m**	**3.25m**	**3.5m**
Pre-stress	6.14	5.63	5.63	6.16	6.15	6.15	5.66
LC1(wind-uplift)	6.05	5.48	5.46	6.07	6.07	6.06	5.46
LC2(snow-load)	6.10	5.61	5.60	6.11	6.10	6.10	5.61
CO1(1.6*LC2)	6.06	5.56	5.53	6.07	6.07	6.06	5.51
CO2(0.5*LC1+1.6LC2)	6.11	5.63	5.62	6.12	6.12	6.11	5.63

The fill stresses development on the other hand are very much inclined with the applied amount of pre-stressing in case of form-finding procedure. On application of 3.0kN/m pre-stressing in fill direction the obtained magnitude of fill stresses after stress deformation analysis is found to be dropping below the applied stress. It is observed from the

Table 12 below that, the fill stresses for height 3.5m is found to be minimum of all the other heights for each load case. The fill stresses closer to 3.0kN/m are observed for the case of 1.5m height of the structure. And it descends slowly as the height of the TMS is increased.

Table 12 The minimum fill/weft stress description of stress-deformation analysis of Hypar TMS (anisotropic stress)

Load cases as per ASCE 7-16	**Minimum fill stress kN/m for variation of height H**						
	1.5 m	**2.0m**	**2.5m**	**2.75m**	**3.0m**	**3.25m**	**3.5m**
Pre-stress	2.97	2.96	2.96	2.965	2.96	2.96	2.95
LC1(wind-uplift)	2.64	2.68	2.58	2.30	2.29	2.28	2.38
LC2(snow-load)	2.77	2.72	2.65	2.63	2.60	2.56	2.50
CO1(1.6*LC2)	2.65	2.56	2.45	2.34	2.32	2.32	2.24
CO2(0.5*LC1+1.6LC2)	2.83	2.79	2.74	2.72	2.69	2.66	2.62

The stress development contours for height 3.5m for both warp and fill are demonstrated in the Figure 24 below. It is observed that the maximum warp stresses are mainly concentrated around the centre of the membrane. The minimum magnitude of fill/weft direction stresses on the other hand are primarily concentrated in the regions between corner and centre of the canopy, and the mid-span of edges are seems to experience minimum fill stress and maximum fill stress too. This an interesting observation about the development of an inflexion point where the condition of minimum and maximum fill stresses occur at the same point. The higher magnitude of the fill stresses are oriented towards the elevated corners and the lower magnitude of fill stress is seems to be lying towards depressed corners of the membrane.

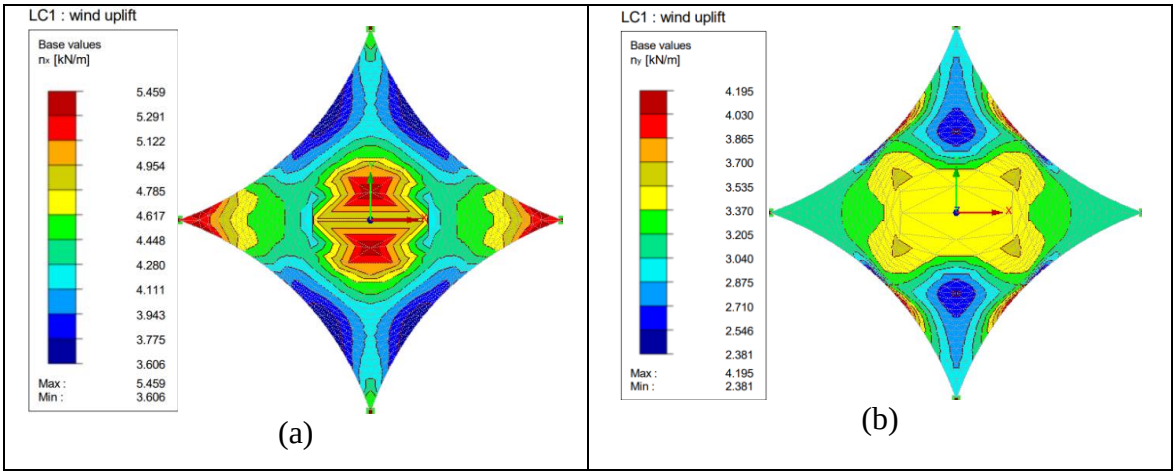

(a) (b)

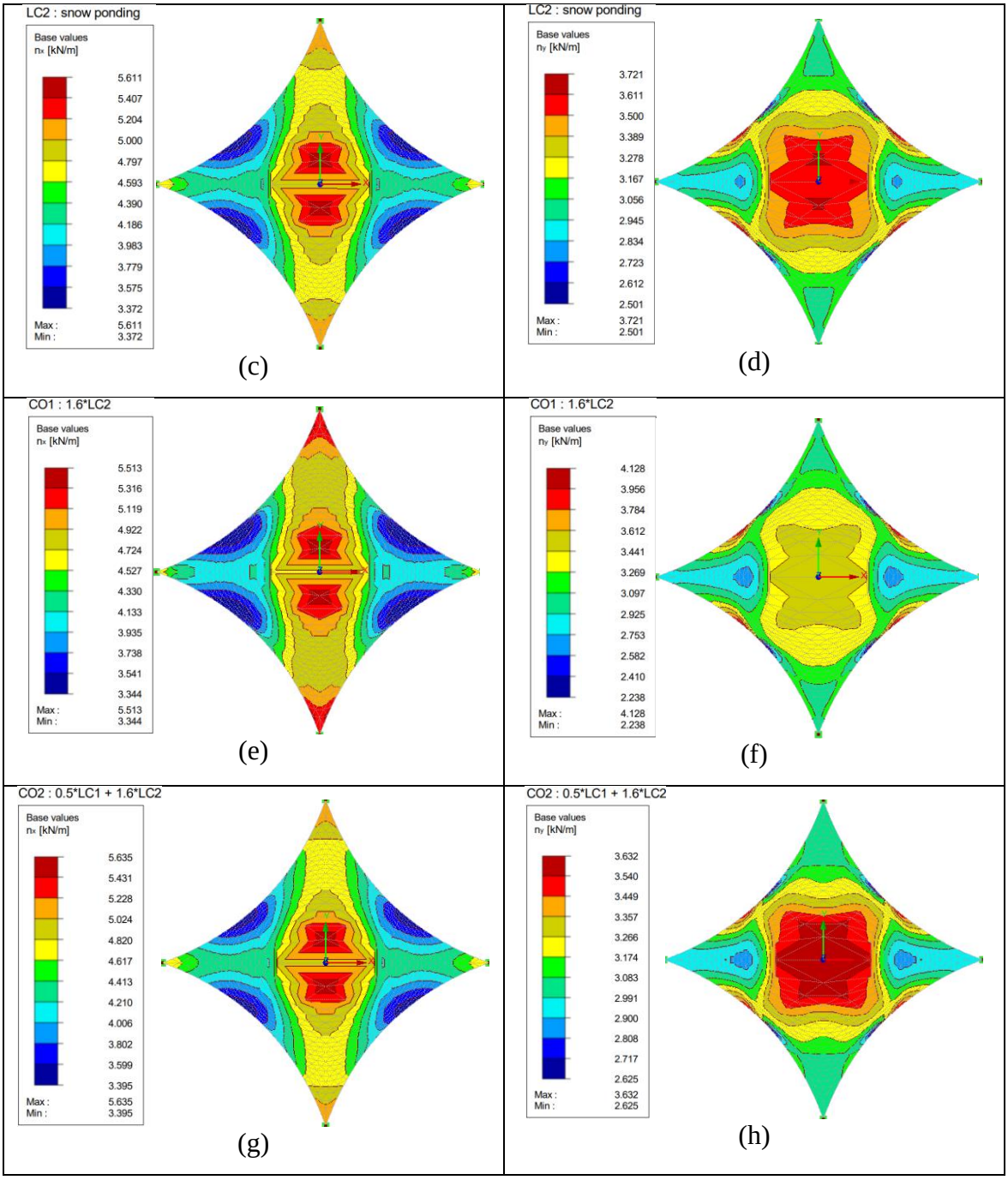

Figure 24 The stress development contours for height 3.5m for both warp and fill direction stresses for Hypar TMS (anisotropic pre-stress)

4.5.4.1 Maximum deformation of TMS due to change in the coefficient of curvature for Anisotropic pre-stressing of hypar shaped TMS.

The deformation analysis for hypar membrane surface under the condition of anisotropic pre-stressing has been tabulated in the Table 13**.** The maximum deformation experienced is 927.2 mm for the load case *LC1*, for height of the structure equals to 3.25 m. The further increment in the height have resulted in the reduction in the deformation to 811.2 mm for the height 3.5m. The deformation for every height have shown a commom trend

of increment in deformation with the height. It increases for every load from height 1.5m to 3.25 m, and then decreases for height case 3.5m for each load case except the form-finding (only pre-stress load applied). In case of form-finding the deformation is maximum for height 3.5m.

As compared to the deformations in the case of isotropic pre-stressing of hypar membrane, the deformations for all the load cases evidences the lower deformations except for the form-finding process. The form finding process in this case experiences relatively high deformations as compared to the isotropic pre-stressing, a detaileddescription of the form-finding in each cases have already been discussed in the section no 4.5.1 and 4.5.2.

Table 13 The maximum z-axis deformation for various load cases with change in height of Hypar TMS (anisotropic pre-stressing)

Load cases as per ASCE	**Variation of the height (H) in m.**						
7-16	**1.5**	**2.0**	**2.5**	**2.75**	**3.0**	**3.25**	**3.5**
Pre-stress	114.2	155.2	171.9	192.3	204.5	215.6	235.0
LC1(wind-uplift)	627.8	645.1	662.7	826.0	877.0	927.2	811.2
LC2(snow-load)	381.6	384.2	405.1	523.9	556.7	590.9	459.3
CO1(1.6*LC2)	602.0	615.1	643.4	797.3	846.6	895.3	727.6
CO2(0.5*LC1+1.6LC2)	296.4	294.5	311.0	409.0	435.5	461.3	353.4

4.5.4.2 The demonstration of deformation contours (Anisotropic Pre-stress)

A detailed visualization of the deformations for different load cases are demonstrated in the form of simulation models and graphical representation in the following section

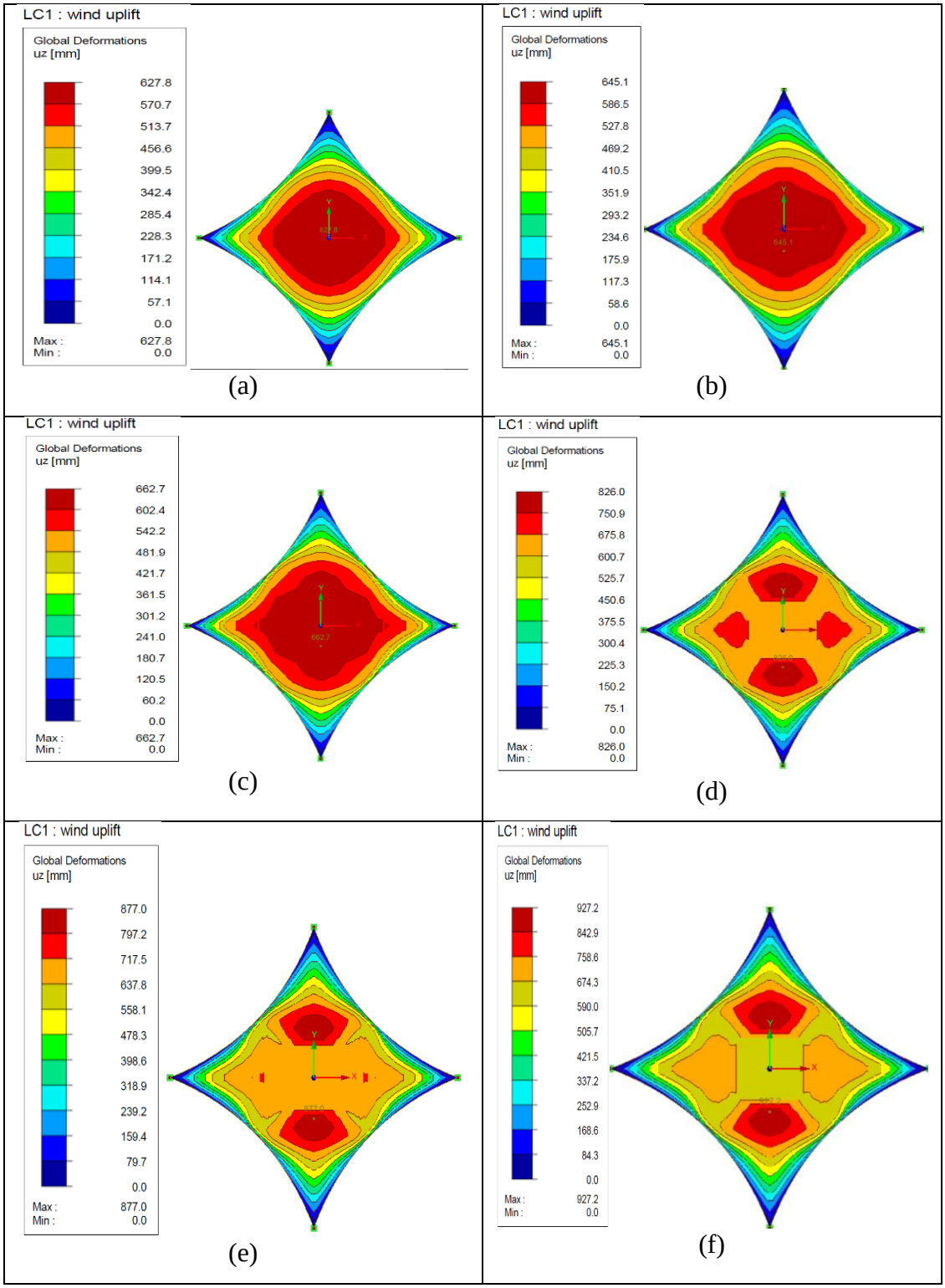

Figure 25 The deformation contour models for wind-uplift load case of Hypar TMS (Anisotropic pre-stress)

The deformation contours for wind uplift load shows the development of a centrally deformed region which is oval in shape for height 1.5m as can be seen from the Figure 26(a). This shape of deformation contours starts distorting with the increase in the height of the structure as distorted oval shape for heights 2.0m and 2.5m depicting the slow rate

of deformation. There is a sudden change in the deformation when the height of TMS is increased to 2.75m, the maximum deformation changes from 662.7mm to 826.0mm. This signifies that the serviceability limit of hypar structure with height 2.75m is less than similar structure with height 2.5m. The shape of deformation contours are also changed, and are seems to be developed towards warp and fill directions as shown in Figure 26 (d). It is also observed that the deformation contours for the greater height are more intense in weft directions when the maximum deformation is recorded higher than 700 mm.

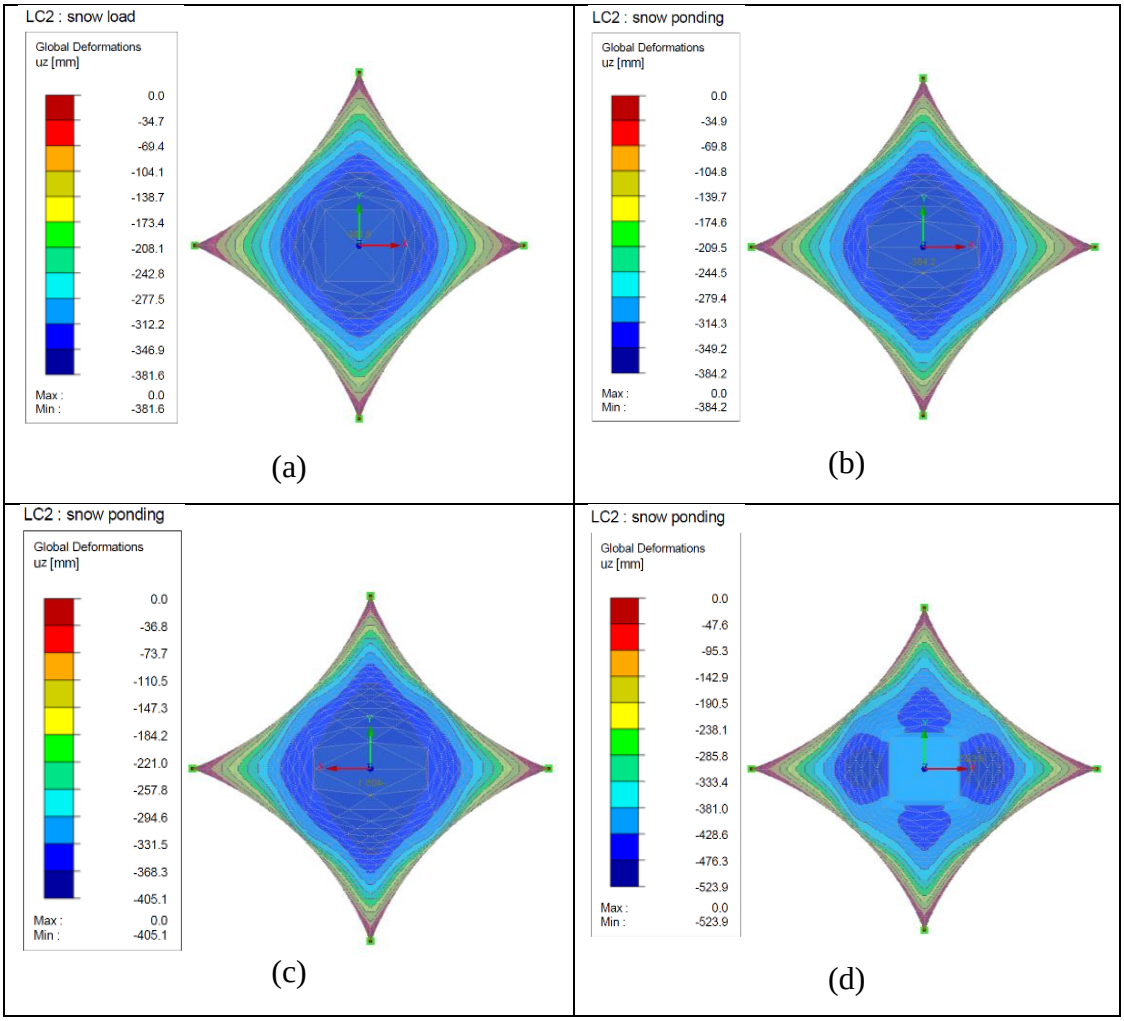

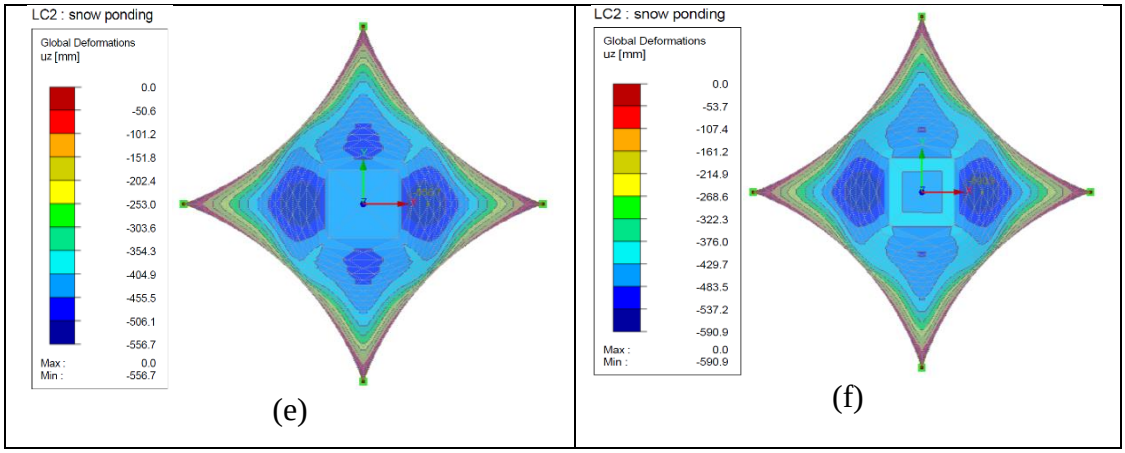

Figure 26 The deformation contour models for snow load case of Hypar TMS (Anisotropic pre-stress)

The deformation pattern in the snow load case is similar to that of wind uplift force as the deformation contours suggests there is a slow increment in the deformations from height 1.5m to 2.5m. There is a fast increment in deformations when the height is increased to 2.75m, and then it declines as the height approaches 3.5m. The development of contours is evidenced from oval shape to localised high magnitude region in the warp and fill directions towards the corners of the hypar TMS. One of the significant point to be noticed is that; unlike wind uplift forces the development of high magnitude deformation takes place along the fill direction and not in weft direction as evidenced in the case of wind uplift load.

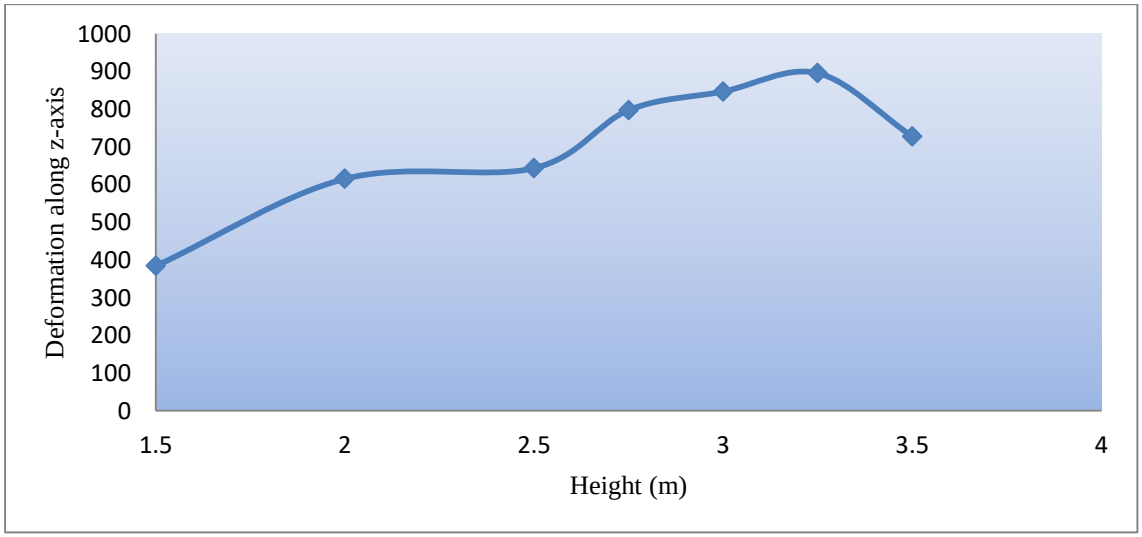

Figure 27 Deformation profile of load case CO1 for Hypar TMS (Anisotropic pre-stress)

The deformation variation in the load cases *CO1* and *CO2* are showing the same pattern as seen in the last two cases. There is a slow rate increase in the deformation from height

1.5m to 2.5m and then it changes fast when height reaches 2.75m and finally there is a decline in deformation as height reaches 3.5m, as can be seen from Figure 28 .

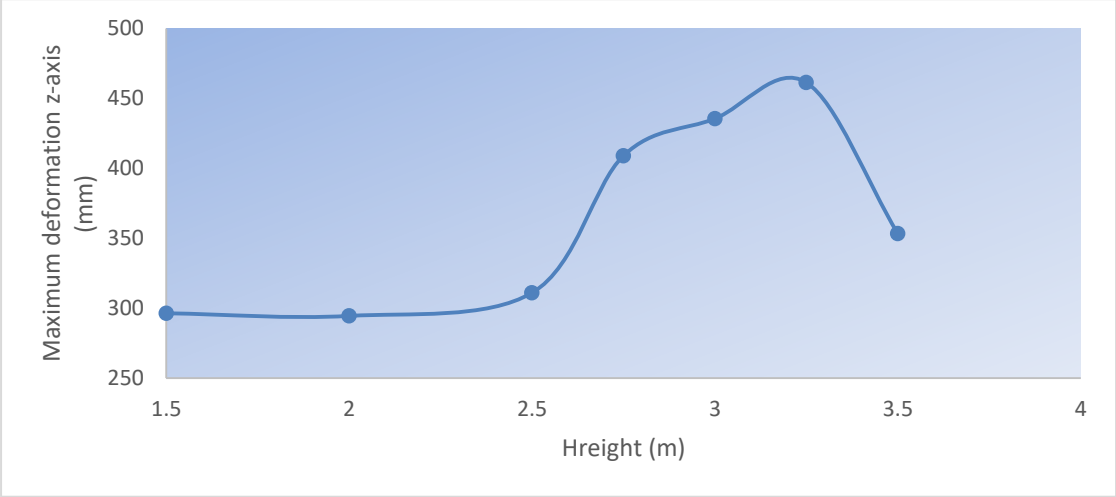

Figure 28 Deformation profile of load case CO2 for Hypar TMS (Anisotropic pre-stress)

The overall outcome of the stress deformation analysis of anisotropic pre-stressed hypar TMS is that the lesser height (upto 2.5m) structures offer better serviceability limit state with respect to similar structures with more height.

4.5.5 Reliability Analysis of hypar TMS

The "limit state" approach involving the strength reduction factor of safety coefficients is one of the widely accepted methodologies to offer an optimal and safe design. This method of analysis is generally regarded as a trade-off between the overall cost and the reliability, due to the obvious reason of utilizing such a high value of safety coefficients. The safety coefficients represent the uncertainty involved with the geometry, loading environment and materials. Unlike traditional structural systems, in the TMS design and analysis the stochasticity in loading induces the high variability in the stress distribution which consequently imparts the highly non-linear behavior to the TMS system. In order to compensate the uncertainties emerging due to load distribution and corresponding material behavior, a permissible stress design methodology is offered in parallel to the limit state design philosophy.

The ultimate material strength of 6.667 kN/m has been implemented in this case. Which is considered as equivalent to an ultimate tensile strength of 40 kN/m of lightweight PVC coated polyester fabric with a stress reduction factor of 6 applied (as per IASS recommendations). In this example the hypar has been subjected to five different loading

conditions along with the variability of overall height (1.5m to 3.5m) of the TMS, hence for the preferred modeling direction the warp stress will always be greater than the fill/weft stress.

The deformation criteria for serviceability limit state is cannot be applied for the adopted limiting values of the deflection limit state, as the deformations in most of the cases are much greater than the prescribed allowable deflection. Only pre-stress implemented for form-finding of the TMS can be judged based on the adopted serviceability deflection limit state criteria.

4.5.5.1 Reliability indices for the fabric failure limit state in case of isotropic prestressing of Hypar TMS

The reliability assessment of the hypar structure starts with the calculation of reliability indices for each height of the structure, subjected to five different types of loading. Initially the coefficient of variance is set as 10% i.e. COV = 0.1. In order to explore the sensitivity of random variables towards the failure probability, the standard deviation is varied from 0.1 to 0.25. The reliability indices with the standard deviation of $\sigma_{permissible}$ from 0.667 kN/m (COV=0.1) to 1.667 kN/m (COV = 0.25) are computed in further section of this chapter. The reliability indices for different loading conditions obtained from the combination of FORM with finite element formulations for fabric failure (ultimate failure), and serviceability limit state. The maximum warp stress values and minimum fill/weft stress values obtained as a stress-deformation response of membrane surface are employed to obtain the reliability indices for both the limit state parameters. The results of reliability analysis are displayed in the Table 14 to Table 17 for fabric failure limit state, and Table 18 to

Table 21 for wrinkling failure limit state of design.

Table 14 Reliability indices for the fabric failure limit state for each load case with COV = 0.10 corresponding to different height of Hypar TMS (Isotropic pre-stress).

Load cases as per ASCE 7-16 National Annex.	**Reliability index for variation of height H**						
	1.5 m	**2.0m**	**2.5m**	**2.75m**	**3.0m**	**3.25m**	**3.5m**
Pre-stress	3.80	3.56	3.42	3.31	3.20	3.12	2.85
LC1(wind-uplift)	2.87	2.63	2.41	2.29	2.24	2.10	1.92

LC2(snow-load)	3.33	3.10	2.88	2.76	2.67	2.55	2.36
CO1(1.6*LC2)	2.97	2.61	2.51	2.38	2.29	2.16	2.07
CO2(0.5*LC1+1.6LC2)	3.67	3.28	3.07	2.95	2.86	2.59	2.48

Table 15 Reliability indices for the fabric failure limit state for each load case with COV = 0.15 corresponding to different height of Hypar TMS (Isotropic pre-stress)

Load cases as per ASCE 7-16	**Reliability index for variation of height H**						
	1.5 m	**2.0m**	**2.5m**	**2.75m**	**3.0m**	**3.25m**	**3.5m**
Pre-stress	2.10	1.98	1.87	1.80	1.72	1.65	1.56
LC1(wind-uplift)	1.50	1.37	1.30	1.13	1.16	1.07	0.89
LC2(snow-load)	1.79	1.64	1.49	1.40	1.32	1.26	1.17
CO1(1.6*LC2)	1.53	1.38	1.24	1.17	1.08	1.01	0.93
CO2(0.5*LC1+1.6LC2)	1.87	1.74	1.59	1.51	1.44	1.32	1.27

Table 16 Reliability indices for the fabric failure limit state for each load case with COV = 0.20 corresponding to different height of Hypar TMS (Isotropic pre-stress)

Load cases as per ASCE 7-16	**Reliability index for variation of height H**						
	1.5 m	**2.0m**	**2.5m**	**2.75m**	**3.0m**	**3.25m**	**3.5m**
Pre-stress	1.32	1.17	1.13	1.05	0.98	0.96	0.88
LC1(wind-uplift)	0.85	0.74	0.63	0.56	0.52	0.45	0.38
LC2(snow-load)	1.05	0.94	0.83	0.76	0.7	0.65	0.57
CO1(1.6*LC2)	0.87	0.75	7.64	0.57	0.62	0.47	0.31
CO2(0.5*LC1+1.6LC2)	1.11	1.04	1.01	0.86	0.79	0.68	0.63

Table 17 Reliability indices for the fabric failure limit state for each load case with COV = 0.25 corresponding to different height of Hypar TMS (Isotropic pre-stress)

Load cases as per ASCE 7-16	**Reliability index for variation of height H**						
	1.5 m	**2.0m**	**2.5m**	**2.75m**	**3.0m**	**3.25m**	**3.5m**
Pre-stress	0.72	0.63	0.58	0.54	0.49	0.45	0.4
LC1(wind-uplift)	0.36	0.27	0.29	0.24	0.19	0.05	0.06
LC2(snow-load)	0.56	0.43	0.32	0.3	0.25	0.2	0.17

CO1(1.6*LC2)	0.38	0.29	0.21	0.16	0.12	0.07	0.03
CO2(0.5*LC1+1.6LC2)	0.58	0.5	0.42	0.37	0.32	0.26	0.21

4.5.5.2 Reliability indices for the wrinkling failure limit state in case of An isotropic pre-stressing of Hypar TMS

The wrinkling failure criteria considered for the serviceability limit state of the hypar TMS is used to obtain the reliability indices corresponding to each height of the structure for the prescribed load cases are displayed in the Table 18 below.

Table 18 Reliability indices for the wrinkling failure limit state for each load case with COV = 0.10 corresponding to different height of Hypar TMS (Isotropic pre-stress)

Load cases as per ASCE 7-16	**Reliability index for variation of height H**						
	1.5 m	**2.0m**	**2.5m**	**2.75m**	**3.0m**	**3.25m**	**3.5m**
Pre-stress	0.59	1.38	1.38	0.56	0.59	0.57	1.34
LC1(wind-uplift)	0.68	1.37	1.40	0.66	0.65	0.65	1.39
LC2(snow-load)	0.62	1.20	1.22	0.60	0.62	0.62	1.20
CO1(1.6*LC2)	0.67	1.27	1.31	0.66	0.66	0.65	1.33
CO2(0.5*LC1+1.6LC2)	0.60	1.18	1.18	0.59	0.59	0.60	1.18

Table 19 Reliability indices for the wrinkling failure limit state for each load case with COV = 0.15 corresponding to different height of Hypar TMS (Isotropic pre-stress)

Load cases as per ASCE 7-16	**Reliability index for variation of height H**						
	1.5 m	**2.0m**	**2.5m**	**2.75m**	**3.0m**	**3.25m**	**3.5m**
Pre-stress	0.39	0.79	0.79	0.37	0.39	0.41	0.83
LC1(wind-uplift)	0.45	0.91	0.96	0.42	0.44	0.44	0.95
LC2(snow-load)	0.41	0.81	0.82	0.41	0.41	0.41	0.81
CO1(1.6*LC2)	0.40	0.84	0.88	0.42	0.42	0.43	0.89
CO2(0.5*LC1+1.6LC2)	0.41	0.79	0.80	0.40	0.40	0.41	0.79

Table 20 Reliability indices for the wrinkling failure limit state for each load case with COV = 0.20 corresponding to different height of Hypar TMS (Isotropic pre-stress)

Load cases as per ASCE 7-16	**Reliability index for variation of height H**						
	1.5 m	**2.0m**	**2.5m**	**2.75m**	**3.0m**	**3.25m**	**3.5m**
Pre-stress	0.29	0.77	0.77	0.28	0.29	0.28	0.73
LC1(wind-uplift)	0.34	0.68	0.70	0.31	0.32	0.32	0.69
LC2(snow-load)	0.31	0.78	0.80	0.30	0.31	0.31	0.78
CO1(1.6*LC2)	0.33	0.64	0.65	0.31	0.31	0.32	0.67
CO2(0.5*LC1+1.6LC2)	0.30	0.77	0.77	0.29	0.29	0.30	0.77

Table 21 Reliability indices for the wrinkling failure limit state for each load case with COV = 0.25 corresponding to different height of Hypar TMS (Isotropic pre-stress)

Load cases as per ASCE 7-16	**Reliability index for variation of height H**						
	1.5 m	**2.0m**	**2.5m**	**2.75m**	**3.0m**	**3.25m**	**3.5m**
Pre-stress	0.23	0.47	0.47	0.22	0.23	0.22	0.45
LC1(wind-uplift)	0.27	0.55	0.57	0.24	0.25	0.25	0.56
LC2(snow-load)	0.24	0.48	0.48	0.23	0.24	0.24	0.48
CO1(1.6*LC2)	0.26	0.50	0.53	0.24	0.24	0.26	0.59
CO2(0.5*LC1+1.6LC2)	0.23	0.46	0.46	0.22	0.22	0.23	0.46

After the reliability assessment of an isotropically pre-stressed hyperbolic paraboloid membrane the results shows very interesting results specially in the variable pre-stressing case. All the random variables being normally distributed with initial standard deviation for each parameter as 10% (COV = 0.10). It offers the value of reliability index for fabric failure in a range around 2.07 to 3.80 as shown in Table 14 for fabric failure limit state and the reliability indices in the range of 0.60 to 1.38 for wrinkling failure limit state as shown in Table 18. The safety index criteria as per Eurocode (Table 1 Table 2) are typically 3.8 for ultimate limit state and the mentioned value for serviceability limit state is 1.5.

The reliability assessment of isotropic pre-stressed hypar TMS suggests that there are a fair chances of the acceptance of the current methodology specially for form-finding case ,where only pre-stressing is applied. The reliability evaluation of form-finding process obtains the reliability index close to 3.8 for most of the adopted height cases except for 3.5m height, and it delivers exactly 3.80 value of reliability index for the height case 1.5m of form finding. The wrinkling failure in the other hand is only acceptable if it is considered as a serviceability fulfillment criteria of the TMS, as all of the reliability indices value are below 1.5.

4.5.5.3 Reliability indices for the fabric failure limit state in case of Anisotropic prestressing of Hypar TMS

The reliability indices calculations for the case of anisotropically pre-stressed hypar TMS are obtained using the adopted methodology. The results show very interesting results and are seems to be in good agreement with the prevailing design recommendations specially for the procedure of form-finding. Table 22, Table 23, Table 24, and Table 25 show the results of reliability indices for the COV variation of 0.10 to 0.25 for the fabric failure limit state for each load case and various height of the anisotropic pre-stressing of hypar TMS.

Table 22 Reliability indices for the fabric failure limit state for each load case with COV = 0.10 corresponding to different height of Hypar TMS (Anisotropic pre-stress)

Load cases as per ASCE 7-16	**Reliability index for variation of height H**						
	1.5 m	**2.0m**	**2.5m**	**2.75m**	**3.0m**	**3.25m**	**3.5m**
Pre-stress	2.58	2.21	2.22	2.56	2.54	1.54	2.15
LC1(wind-uplift)	1.68	2.37	2.40	1.65	1.65	1.67	2.40
LC2(snow-load)	1.62	2.22	21.31	1.61	1.62	1.62	2.28
CO1(1.6*LC2)	1.67	2.27	2.31	1.65	1.65	1.67	2.36
CO2(0.5*LC1+1.6LC2)	1.61	2.22	2.24	1.63	1.63	1.61	2.22

Table 23 Reliability indices for the fabric failure limit state for each load case with COV = 0.15 corresponding to different height of Hypar TMS (Anisotropic pre-stress)

Load cases as per ASCE 7-16	**Reliability index for variation of height H**						
	1.5 m	**2.0m**	**2.5m**	**2.75m**	**3.0m**	**3.25m**	**3.5m**

Pre-stress	0.38	0.79	0.79	0.37	0.35	0.35	0.76
LC1(wind-uplift)	0.45	0.92	0.93	0.43	0.43	0.45	0.93
LC2(snow-load)	0.41	0.81	0.82	0.40	0.41	0.41	0.81
CO1(1.6*LC2)	0.44	0.85	0.87	0.42	0.42	0.44	0.91
CO2(0.5*LC1+1.6LC2)	0.40	0.79	0.80	0.38	0.38	0.40	0.79

Table 24 Reliability indices for the fabric failure limit state for each load case with COV = 0.20 corresponding to different height of Hypar TMS (Anisotropic pre-stress)

Load cases as per ASCE 7-16	**Reliability index for variation of height H**						
	1.5 m	**2.0m**	**2.5m**	**2.75m**	**3.0m**	**3.25m**	**3.5m**
Pre-stress	0.29	0.59	0.59	0.27	0.28	0.28	0.58
LC1(wind-uplift)	0.34	0.69	0.71	0.32	0.32	0.33	0.71
LC2(snow-load)	0.31	0.60	0.61	0.30	0.31	0.31	0.60
CO1(1.6*LC2)	0.33	0.63	0.65	0.32	0.32	0.33	0.72
CO2(0.5*LC1+1.6LC2)	0.30	0.59	0.69	0.31	0.31	0.30	0.59

Table 25 Reliability indices for the fabric failure limit state for each load case with COV = 0.25 corresponding to different height of Hypar TMS (Anisotropic pre-stress)

Load cases as per ASCE 7-16	**Reliability index for variation of height H**						
	1.5 m	**2.0m**	**2.5m**	**2.75m**	**3.0m**	**3.25m**	**3.5m**
Pre-stress	0.23	0.47	0.47	0.21	0.22	0.22	0.45
LC1(wind-uplift)	0.27	0.55	0.57	0.24	0.24	0.25	0.59
LC2(snow-load)	0.26	0.48	0.49	0.24	0.26	0.26	0.48
CO1(1.6*LC2)	0.27	0.51	0.54	0.27	0.27	0.27	0.56
CO2(0.5*LC1+1.6LC2)	0.24	0.47	0.47	0.24	0.24	0.24	0.47

4.5.5.4 Reliability indices for the wrinkling failure limit state in case of An isotropic pre-stressing of Hypar TMS

The results of reliability indices corresponding to wrinkling failure limit state of hypar TMS (anisotropic pre-stress) are demonstrated in Table 26 to Table 29. The results show

good agreement with the existing design code based safety index values see. Table 1 and Table 2.

Table 26 Reliability indices for the wrinkling failure limit state for each load case with COV = 0.10 corresponding to different height of Hypar TMS (Anisotropic pre-stress)

Load cases as per ASCE 7-16	**Reliability index for variation of height H**						
	1.5 m	**2.0m**	**2.5m**	**2.75m**	**3.0m**	**3.25m**	**3.5m**
Pre-stress	2.06	2.08	2.08	2.08	2.08	2.08	2.07
LC1(wind-uplift)	1.76	1.80	1.68	1.41	1.35	1.32	1.48
LC2(snow-load)	1.86	1.82	1.74	1.71	1.69	1.66	1.58
CO1(1.6*LC2)	1.77	1.67	1.56	1.44	1.42	1.42	1.26
CO2(0.5*LC1+1.6LC2)	2.01	1.88	1.84	1.82	1.81	1.77	1.71

Table 27 Reliability indices for the wrinkling failure limit state for each load case with COV = 0.15 corresponding to different height of Hypar TMS (Anisotropic pre-stress)

Load cases as per ASCE 7-16	**Reliability index for variation of height H**						
	1.5 m	**2.0m**	**2.5m**	**2.75m**	**3.0m**	**3.25m**	**3.5m**
Pre-stress	1.86	1.86	1.88	1.88	1.88	1.88	1.87
LC1(wind-uplift)	1.56	1.61	1.48	1.21	1.15	1.13	1.28
LC2(snow-load)	1.64	1.60	1.52	1.59	1.47	1.45	1.36
CO1(1.6*LC2)	1.57	1.46	1.35	1.23	1.21	1.21	1.05
CO2(0.5*LC1+1.6LC2)	1.81	1.67	1.62	1.60	1.58	1.56	1.51

Table 28 Reliability indices for the wrinkling failure limit state for each load case with COV = 0.20 corresponding to different height of Hypar TMS (Anisotropic pre-stress)

Load cases as per ASCE 7-16	**Reliability index for variation of height H**						
	1.5 m	**2.0m**	**2.5m**	**2.75m**	**3.0m**	**3.25m**	**3.5m**
Pre-stress	1.35	1.35	1.37	1.37	1.37	1.37	1.36
LC1(wind-uplift)	1.25	1.30	1.17	0.90	0.84	0.82	0.94
LC2(snow-load)	1.39	1.35	1.19	1.24	1.12	1.10	1.01
CO1(1.6*LC2)	1.25	1.14	1.03	0.91	0.89	0.89	0.73
CO2(0.5*LC1+1.6LC2)	1.50	1.36	1.31	1.30	1.20	1.26	1.20

Table 29 Reliability indices for the wrinkling failure limit state for each load case with COV = 0.25 corresponding to different height of Hypar TMS (Anisotropic pre-stress)

Load cases as per ASCE 7-16	**Reliability index for variation of height H**						
	1.5 m	**2.0m**	**2.5m**	**2.75m**	**3.0m**	**3.25m**	**3.5m**
Pre-stress	0.95	0.95	0.97	0.97	0.97	0.97	0.96
LC1(wind-uplift)	0.85	0.90	0.77	0.51	0.42	0.41	0.54
LC2(snow-load)	0.99	0.95	0.79	0.84	0.72	0.70	0.61
CO1(1.6*LC2)	0.85	0.74	0.63	0.51	0.48	0.48	0.33
CO2(0.5*LC1+1.6LC2)	1.05	0.91	0.86	0.85	0.76	0.81	0.76

The results of fabric failure limit state based reliability index are obtained to be in the range of 1.61 to 2.58 which is subsequently does not meet the ultimate failure criteria of safety index 3.8. This is because of the fact that the obtained warp stresses from section 4.5.4 are approaching the allowable limiting value of 6.77kN/m. The serviceability limit state using wrinkling criteria obtains good results fulfilling the design requirement criteria of having safety index above 1.5 as can be seen from Table 26 all the β values for each load case and corresponding height if falling around and above 1.5.

4.6 Summary

In this chapter a novel finite element based probabilistic design approach is highlighted by implementing it to the simple and realistic hypar TMS. Based on the obtained results from the form –finding analysis and stress-deformation analysis, it can be clinched that the current design approach is a well versed methodology for form-finding both isotropic and anisotropic pre-stressed hypar TMS. For stress deformation analysis it is proven to be suitable for isotropically pre-stressed hypar TMS, in case of anisotropic pre-stressing the maximum surface obtained stresses are observed to be exceeding the allowable stresses.

The FORM obtained reliability indices for both the cases show satisfying results. The fabric failure limit state based criteria implementing the ultimate tensile strength of the fabric material and curing it with the help of stress reduction factors meant to contain the uncertainty involved in the material behavior in response to the external loads. For isotropic pre-stressing of hypar TMS the method proves to be fulfilling the ultimate failure criteria and lacking behind to meet the serviceability requirement of the structure.

In contrary to that the anisotropic pre-stressing of hypar TMS is well evaluated for serviceability failure criteria, and doesn’t meet the fabric failure limit state of design.